POLITECNICO DI MILANO

School of Industrial and Information Engineering

Master of Science in Engineering Physics

Simulation of Montel system

Supervisor: Prof. Giacomo GHIRINGHELLI

Assistant supervisor: Dr. Manuel SANCHEZ DEL RIO

Candidate:

Yiones AOUADI   872727

Academic Year 2017 - 2018

The whole work presented in these pages was carried out at the European Synchrotron Radiation Facility (ESRF), in Grenoble, under the supervision of dr. M. Sanchez del Rio.

Contents

List of Figures

List of Tables

Sommario

La simulazione delle proprietà di fasci di raggi X lungo la propagazione nelle beamline, è uno step importante per la progettazione e l'ottimizzazione di esse. Per sistemi ottici basati sulla riflessione singoli specchi o particolari combinazioni di specchi vengono utilizzati per la focalizzazione del fascio. Un esempio tipico di questi sistemi è il sistema KirckPatrick-Baez (KB), molto popolare all'ESRF per le sue molteplici qualità. Comunque, siccome la qualità dei fasci generata dal sincrotrone dell'ESRF è molto elevate, si va sempre più alla ricerca di elementi ottici via via migliori.

Durante il mio periodo di tirocinio all'ESRF, ho sviluppato una libreria python, in grado di simulare la propagazione di fasci attraverso semplici specchi sferici, e combinazioni di essi quali il sopracitato KirckPatrick-Baez e un altro sistema, denominato Montel. Lo scopo della tesi è stato quello di studiare il sistema Montel utilizzando la libreria generata per poi implementarla nel software OASYS.

Abstract

The simulation of x-ray beam properties during the transport along a beamline is important for the design, the optimization and the operation of the beamline. For reflection optical system single mirrors or particular combination of them are used to increase the focusing property of a beam. A typical example is the Kirkpatrick-Baez (KB) system, very popular at the ESRF because of its many good properties and so well studied. However, the extreme quality of the synchrotron beams that will be available with the ESRF upgraded storage ring pushes the requirement in optics to consider more and more perfect elements.

During my traineeship period at ESRF, I developed a python library in able to simulate a beam propagation along simple surface conic mirrors, and combination of them such as the already discussed KirckPatrick-Baez and another system, named Montel. The aim of the thesis was that to study the effect of Montel system using the built library to then implement it in OASYS.

Introduction

The simulation of x-ray beam properties during the transport along a beamline is important for the design, the optimization and the operation of the beamline. For X-ray radiation both refractive and reflective elements are used. But, in this thesis, is discussed only the reflection optics (mirrors and combination of them). The aim of the optical system is that to propagate the radiation from the synchrotron source to the sample. This implies some form of focusing on the Beam.
Reflective elements that can focus must be curved mirrors or combination of them. Moreover, because of the high absorption coefficient of the X-ray radiation, a total external reflection is needed. This means that the mirrors are used in a grazing configuration.
The simplest curved mirror existing, spherical one, cannot be used, due to the fact that, at grazing incidence, the image is aberrated a lot. To overcome these aberrations other kinds of curved mirrors can be used: toroidal or conical mirrors. Simple mirror make a good point-to-point focus. In case of an image it needs an "imaging system" that can propagate the radiation in the correct way. System that are able to do this are: Wolter [Wol75], Kirkpatrick-Baez [KB48] and Montel [Mon57] system.
Wolter system are very used in astronomical field. Kirkpatrick-Baez system are very popular at the ESRF because of many good properties. Montel system are not used at ESRF but it is possible to find them in other synchrotron.
OASYS (OrAnge SYnchrotron Suite) [RdR17b] [dRRD$^+$14] is an open-source graphical environment for optic simulation developed by Manuel Sanchez del Rio and Luca Rebuffi. This software is used for optical simulation, in particular for syncrotron radiation, at ESRF and over the facilities around the world. It puts together several packages that allow a user-friendly simulation from the ray tracing tool SHADOW. In this software are already implemented many kinds of optical element such as curved mirrors, KB system and others (both refractive and reflective elements).
During my traineeship I developed a python library MONWES (Montel and Wolter of yunEs), that perform ray tracing simulation for X-ray radiation along system consisting of one or several mirrors. It is implemented also "imaging system" such as Kirkpatrick and Montel system. The aim of this library is to integrate the Montel optical element in OASYS. All the optical elements implemented, apart from Montel system, use a sequential tracing method. This method doesn't work for Montel so more effort was done in its tracing method. I hope that my efforts will help the scientific community on its job.
In the last part of my traineeship I did a simulation work for the beamline ID20. The simulation were done on a Montel used as analyser that the beamline meant

to buy. Comparing the information provided by the company with my simulation. This study is reported in the thesis.

The thesis is divided in 4 Chapters with the following structure:

1. Chapter 1: review of the interaction X-ray - matter in order to explain the importance of the mirror in a grazing configuration to focus and collimate X-ray radiation.

2. Chapter 2: it is reported the geometrical focusing explanation of mirrors. A study of the Kirkpatrick-Baez and Montel system. Moreover, a comparison between them is presented.

3. Chapter 4: describes the models and algorithm implemented in MONWES. And show examples of operation of the program.

4. Chapter 5: a first testing part against OASYS to show the correct work of MONWES. Benchmarking against some results found in bibliography is done. Then it is reported the calculation done with MONWES for an analyser to be installed at the ID20 beamline.

Chapter 1

Focusing for X-rays

Image formation by an optical system usually implies some form of focusing. Moreover, the environment in which the radiation its surrounded, such as the material of which a certain mirror is made, controls the focusing property. In case of the visible light the focusing elements mainly used are lenses with their laws, well-known and studied, for the electron focusing, the optical element become electric and magnetic fields that to curve the path of the electrons. To study the focusing property of the X-ray radiation, it has to consider the interaction that acts between the radiation and the matter. These phenomena are, that rule the interaction radiation-matter are:

1. elastic scattering;

2. inelastic scattering;

3. scattering via photoelectric effect.

The first effect, where there is an exchange of energy, is constituted by: Thomson scattering, that it is the scattering of electromagnetic radiation by a free non relativistic charged particle [Dal16], and Rayleigh scattering, an elastic scattering between the radiation and the strongly bounded electrons that act cooperatively [Fit06]. Because, the elastic scattering, generated a defined phase relation between the incident and the scattered radiation, it is the responsible for Bragg diffraction. The second effect, inelastic scattering, or Compton scattering [Uni16], that occurs when an electron lost by the atom interact with the radiation and absorb a small energy from the X-ray radiation. This scattering is an incoherent effect so there isn't any phase relation between incident and scattered radiation, moreover the atom pass to another quantum state due to the energy absorbed by the electron. The last effect, absorption via photoelectric effect, occur when a bounded electron with an atom get the necessary energy to break the bound and become free (ionization process). This last phenomenon is the most important effect for the energies of interest at ESRF, i.e. $-keV$. Figure 1.1 show the contribution for the attenuation coefficient, of the different absorption of a light material (water Figure 1.1a), and a heavy material (lead 1.1b) (from [SFV09].
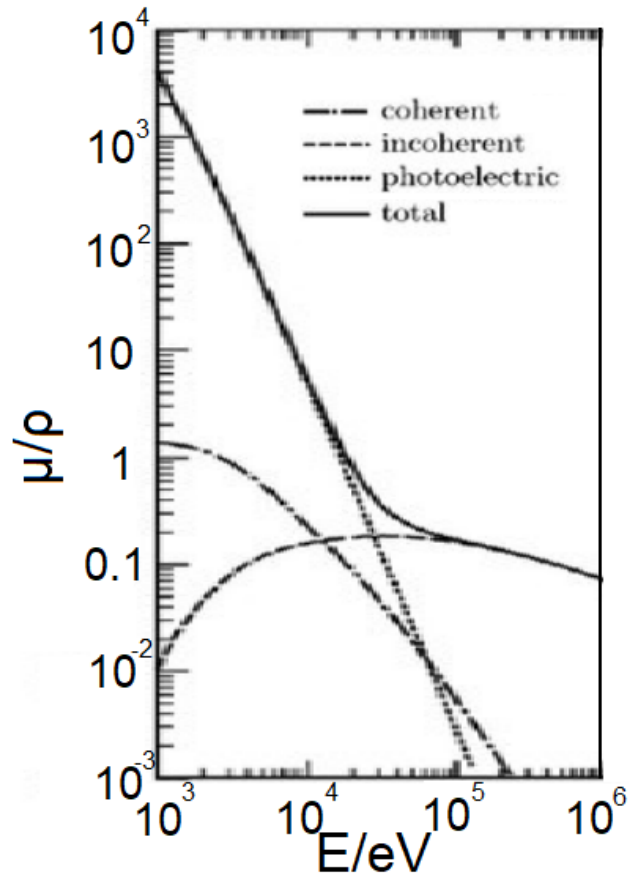
(a) H_2O
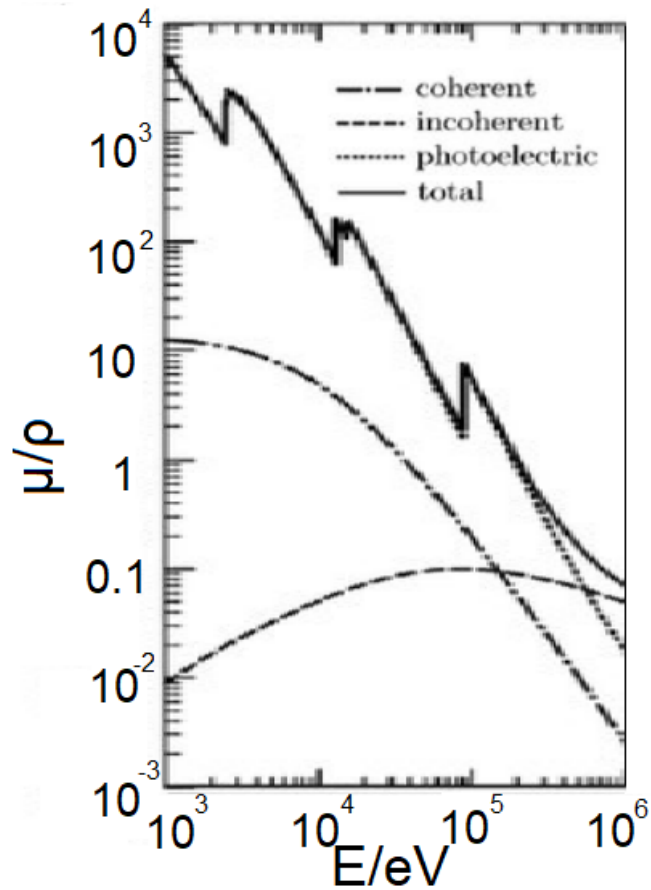
(b) Pb

Figure 1.1: Attenuation coefficient for X-ray radiation of a light material (water Figure 1.1a), and a heavy material (lead 1.1b) (from [SFV09]).

1.1 Interaction with Matter

Interaction between radiation and matter can be compressed in a coefficient (absorption coefficient)), that rule the attenuation of an incident radiation

$$I = I_0 exp(-\mu x) \tag{1.1}$$

where x is the thickness of the material, μ is the absorption coefficient, and I_0 the initial intensity of the beam corresponding to the intensity at $x = 0$. Considering the beam as a plane wave, it is possible to express the amplitude of the electromagnetic wave as:

$$A = A_0 exp(\frac{-2\pi\beta x}{\lambda}) exp(\frac{-2\pi i((1-\delta)x - ct)}{\lambda}) \tag{1.2}$$

where x is the position of the front wave, λ correspond to the wavelength of the wave in the vacuum, δ is a number that describe the dispersive aspect of the wave-matter interaction, and β is the absorption coefficient that describe the absorption aspect of the wave-matter interaction. The propagation of the radiation depends on the complex refractive index n, that can be expressed as:

$$n = 1 - \delta - i\beta \tag{1.3}$$

For X-rays process, the absorption term is the leading term, this mean that the μ coefficient can be defined as linearly dependent from the absorption coefficient, where:

$$\alpha = \frac{4\pi\beta}{\lambda} \tag{1.4}$$

Normally the absorption values tabulated are given are the mass absorption coefficients μ_m, where

$$\mu = \mu_m \rho \tag{1.5}$$

where ρ is the density of the material. The mass absorption of a compound is given by

$$\mu_{m,com} = \sum_j w_j \mu_{m,j} \tag{1.6}$$

where $\mu_{m,j}$ is the mass absorption of a particular element, and w_j is the fraction of the j element in the material. The relation between the absorption coefficient of the material and the mass absorption coefficient is:

$$\alpha_{com} = \mu_{m,com}\rho_{com} \tag{1.7}$$

where ρ_{com} is the density of the compound.
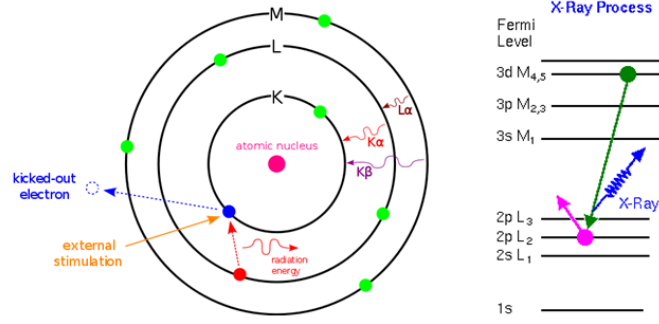
Figure 1.2: X-ray ionizing process

Because of the dominant energy of the radiation with respect to the matter energies involved in the interaction (X-rays energies spreads from 100eV, soft X-ray, to 10keV, hard X-ray, binding and molecular energies are of the order of few eV), the ionization process, as said before, is the leading process in the absorption coefficient. In this case the greater part of the energies involved is transferred to the kinetic term of the ionized electrons. Electron in atom have a well-defined state of energies, so, to be absorbed, the radiation must have at least an energy equal to an electron state energies. For energies equal to the electron state energies, as showed in Figure 1.1, absorption edges appears. The nomenclature $K, L, , M$, of those edges, that are not important for our treatment, correspond to, as it is showed in Figure 1.2, the energies of an electron that goes down from a greater level, for example $n = 2$ to a lower one $n = 1$ ([Aga91]). In reality, the edges, are less pronunciation as the ones in figure, due to the finite energy width of the states, and because of the environment effect.

To understand better the absorption of the X-ray radiation it is reported a brief theoretical treatment of the interaction, because the result are useful for the design of the optical element used for X-rays. The calculation start from the elastic scattering between X-ray photon against free electron (Thomson scattering). The electro-magnetic radiation is characterized by an electric field with amplitude A_0 that accelerate a free electron (of charge e and mass m_e) by an amount of $A_0(e/m)$. A charged particle that is accelerated emits radiation, this change the value of the amplitude of the electric field equal to:

$$A_T(\Phi) = \frac{e}{4\pi\varepsilon_0 c^2 \mathbf{r}}\mathbf{a}\sin\Phi \tag{1.8}$$

where r is the distance from the charge, Φ correspond to the angle between the position vector $\mathbf{r}$ and acceleration vector $\mathbf{a}$. Replacing $\mathbf{a}$ with $A_0(e/m)$:

$$A_T(\Phi) = A_0\frac{e^2}{4\pi\varepsilon_0 c^2 \mathbf{r}}\sin\Phi \tag{1.9}$$

To treat the interaction between the bounded electron and the radiation, going beyond the Thomson scattering, it is possible to multiply the Thomson amplitude $A_T(\Phi)$ to a complex number $f = f_1 + if_2$ named complex atomic scattering. Thus:

$$A(\Phi, E) = A_t(\Phi) * f(E) = A_T(\Phi)[f_1(E) + if_2(E)] \tag{1.10}$$

where the two function f_1 and f_2, depend on the energy of the incident X-ray radiation that, to a first approximation, are independent of the angle between the incident and the scattered radiation ϑ. This approximation has sense because the typical radiation length ($\sim 0.1 - 10nm$) is much larger than the typical length of the atomic electronic distribution ($\sim 1 - 50pm$), the consequence of this approximation is the possibility to consider a phase scattering of the atomic wave function. The values of the two function f_1 and f_2 are calculated in the relativistic quantum dispersion theory [CL70] and are given by:

$$f_1(E) = Z + 4\frac{\varepsilon_0 m_e c}{he^2} \int_0^{+\infty} \frac{W^2 \sigma(W)}{E^2 - W^2} dW - \Delta_{rel} \tag{1.11}$$

and

$$f_2(E) = 2\frac{\varepsilon_0 m_e c}{h} E\sigma(E) \tag{1.12}$$

In Equation 1.11, the first term correspond to the Thomson scattering, where Z correspond to the atomic number of the atom. To add the angle-dependence of the scattering it is used the factor:

$$f_0 = \int_0^{+\infty} U(r) sinc\left[\frac{4\pi r}{\lambda} \sin\frac{\vartheta}{2}\right] dr \tag{1.13}$$

where $U(r)$ represent the radial charge distribution and $sinc(x)$ is the cardinal sine function $= \frac{\sin x}{x}$. Considering a wavelength λ of the order of nanometres, if $\sin\frac{\vartheta}{2} \leq \frac{\lambda}{2}$, $f_0 = Z$, otherwise for $\sin\frac{\vartheta}{2} = \lambda$, typically, for most element $f_0 \simeq 0.9Z$.

In Equation 1.11, the second term (the anomalous dispersion integral), represent the oscillation of the electron after the interaction with the radiation, this can be obtained treating the semi-classically the problem. This approach neglects the damping, so, near the absorption edges $f1$ is inaccurate. The second term of the Equation 1.11, and in Equation 1.12 contain σ that is the photo ionization cross section expressed in $m^2 atom^{-1}$, a coefficient that is related to the mass absorption coefficient in this way:

$$\sigma(E) = A\frac{\mu}{N_0} \tag{1.14}$$

where A is the atomic weight and N_0 the Avogadro's number ($N_0 = 6.22 10^{23} particle mol^{-1}$). The value of $\sigma(E)$ is theoretically obtained knowing the atomic wave function of the atom, so, only for hydrogen it possible to have the correct value, for all the other system, the calculation can be done with approximation methods that give some uncertainty on $\sigma(E)$, consequently on the value of f_1 and f_2.

In Equation 1.11 the third term take in account the relativistic effect. This correction is given by [CL70]:

$$\Delta_{rel} = \frac{5}{3}\frac{|E_{tot}|}{m_e c^2} + \frac{Z}{2}\left(\frac{E}{m_e c^2}\right)^2 \tag{1.15}$$

where $|E_{tot}|$ is the modulus of the total energy of the atom (that is negative), moreover, this third term is the less relevant in Equation 1.11, for X-ray energies, so it is possible to neglect it in the calculation.

For photo absorption event by an electron bounded to an atom, far from the absorption edges, a good approximation is to consider the solid state environment distorted by the ionization of the electrons, because, the most affected electrons are the outer ones. After some calculation, is possible to relate the factors f_1 and f_2 with the macroscopic parameters n and β:

$$\delta = 1 - n = \frac{e^2\hbar^2}{2\varepsilon_0 m_e E^2}\overline{f_1} \tag{1.16}$$

and

$$\beta = \frac{e^2\hbar^2}{2\varepsilon_0 m_e E^2}\overline{f_2} \tag{1.17}$$

where $\overline{f_1}$ and $\overline{f_2}$ are defined as follow:

$$\overline{f_1} = \sum_j N_j f_{1j} \qquad \overline{f_2} = \sum_j N_j f_{2j} \tag{1.18}$$

and represent the average scattering factor per unit volume, N_j is the total number of the particular j element per unit volume. Putting everything together Equation 1.16, apart near the absorption edges, can be expressed as:

$$\delta = \frac{Ne^2\hbar^2}{2\varepsilon_0 m_e E^2}\overline{f_1} = \frac{Ne^2\lambda^2}{8\pi^2\varepsilon_0 m_e c^2}\overline{f_1} \tag{1.19}$$

where N is the number of electrons per unit volume. For X-ray energies the value of δ is small (typically $\sim 10^{-3}$) and positive, this is important because it means that, for X-rays, the refractive index is a bit less than 1. It is possible to find the tabulated values of f_1 and f_2, [?], that are the main ingredient to calculate the curve in Figure 1.1 and these were used to generate Figure 1. This values, according to the experimental results, allow writing, far from absorption edges, the absorption coefficient β such as:

$$\beta \sim Z^2\lambda^3 \tag{1.20}$$

This mean that increasing the photon energy, the absorption decrease, and is it consistent with Figure 1.1, far from the edges. Moreover, the absorption, become bigger with the element used in the optical element, heavy elements absorb more than light elements. This is the reason why, to use refractive lenses for x-ray radiation, one of the used material is the Beryllium.
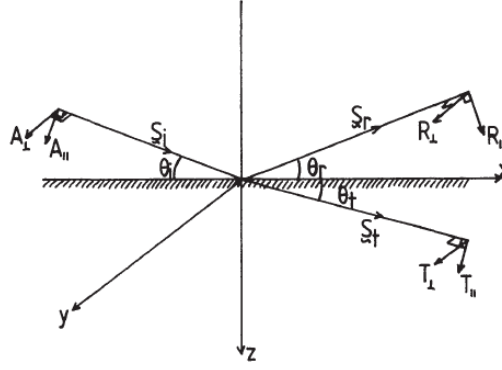
Figure 1.3: Interface of two medium

1.2   Total External Reflection

For the system in Figure 3.15, there are two complex refractive indexes:

$$\overline{n_1} = 1 - \delta_1 - i\beta_1 = n_1 - i\beta_1 \tag{1.21}$$

and

$$\overline{n_2} = 1 - \delta_2 - i\beta_2 = n_2 - i\beta_2 \tag{1.22}$$

moreover $\delta_2 > \delta_1$. In the general case there are, as shown in Figure 3.15 a reflected and a transmitted wave. For the theoretical treatment, initially, will be neglect the absorption ($\beta_1 = \beta_2 = 0$), moreover the permeability coefficient it is supposed to be similar to the permeability in the vacuum. Thus, the law of Snell, can be expressed such as:

$$\frac{\cos \vartheta_i}{\cos \vartheta_t} = \frac{1 - \delta_2}{1 - \delta_1} \tag{1.23}$$

Using the frame system as in Figure 3.15, with the z-axis that correspond to the normal of the interface. It is possible to write the component of the electric field of the waves in this way

$$E_{ix} = A_\parallel \sin \vartheta_i \exp^{-i\tau_i}, \quad E_{iy} = A_\perp \exp^{-i\tau_i}, \quad E_{iz} = A_\parallel \cos \vartheta_i \exp^{-i\tau_i} \tag{1.24a}$$

$$E_{tx} = -T_\parallel \sin \vartheta_t \exp^{-i\tau_t}, \quad E_{ty} = T_\perp \exp^{-i\tau_t}, \quad E_{tz} = T_\parallel \cos \vartheta_t \exp^{-i\tau_t} \tag{1.24b}$$

$$E_{rx} = R_\parallel \sin \vartheta_r \exp^{-i\tau_r}, \quad E_{ry} = R_\perp \exp^{-i\tau_r}, \quad E_{rz} = R_\parallel \cos \vartheta_r \exp^{-i\tau_r} \tag{1.24c}$$

where

$$\tau_i = \omega(t - \frac{\mathbf{r} \bullet \mathbf{s_i}}{v_1}) = \omega \left[t - \frac{(1 - \delta_1)(x \cos \vartheta_i + z \sin \vartheta_i)}{c} \right] \tag{1.25a}$$

$$\tau_t = \omega(t - \frac{\mathbf{r} \bullet \mathbf{s_t}}{v_2}) = \omega \left[t - \frac{(1 - \delta_2)(x \cos \vartheta_t + z \sin \vartheta_t)}{c} \right] \tag{1.25b}$$

$$\tau_r = \omega(t - \frac{\mathbf{r} \bullet \mathbf{s_r}}{v_1}) = \omega \left[t - \frac{(1 - \delta_1)(x \cos \vartheta_r + z \sin \vartheta_r)}{c} \right] \tag{1.25c}$$

where ω is the angular frequency of the wave, and v_1, v_2, correspond to the velocities of propagation that depend on the material as follows:

$$v_1 = \frac{c}{1 - \delta_1}, \quad v_2 = \frac{c}{1 - \delta_2} \tag{1.26}$$

the related magnetic field are:

$$H_{ix} = -A_\perp(1 - \delta_1)\sin\vartheta_i \exp^{-i\tau_i}, \quad H_{iy} = -A_\parallel(1 - \delta_1)\exp^{-i\tau_i},$$
$$H_{iz} = A_\perp(1 - \delta_1)\cos\vartheta_i \exp^{-i\tau_i} \tag{1.27a}$$

$$H_{tx} = -T_\perp(1 - \delta_2)\sin\vartheta_t \exp^{-i\tau_t}, \quad H_{ty} = -T_\parallel(1 - \delta_2)\exp^{-i\tau_t},$$
$$H_{tz} = T_\perp(1 - \delta_2)\cos\vartheta_t \exp^{-i\tau_t} \tag{1.27b}$$

$$H_{rx} = -R_\perp(1 - \delta_1)\sin\vartheta_r \exp^{-i\tau_r}, \quad H_{ry} = -R_\parallel(1 - \delta_1)\exp^{-i\tau_r},$$
$$H_{rz} = R_\perp(1 - \delta_1)\cos\vartheta_r \exp^{-i\tau_r} \tag{1.27c}$$

the boundary condition impose the continuity of the fields:

$$E_{ix} + E_{rx} = E_{tx}, \quad E_{iy} + E_{ry} = E_{ty} \tag{1.28}$$

and

$$H_{ix} + H_{rx} = H_{tx}, \quad H_{iy} + H_{ry} = H_{ty} \tag{1.29}$$

because of Snell's laws $\vartheta_r = \vartheta_t$, so, from the Equation 1.28 and Equation 1.29:

$$(A_\parallel - R_\parallel)\sin\vartheta_i = T_\parallel \sin_t \tag{1.30a}$$

$$A_\perp + R_\perp = T_\perp \tag{1.30b}$$

$$(1 - \delta_1)(A_\perp - R_\perp)\sin\vartheta_i = (1 - \delta_2)T_\perp \sin\vartheta_t \tag{1.30c}$$

$$(1 - \delta_1)(A_\parallel + R_\parallel) = (1 - \delta_2)T_\parallel \tag{1.30d}$$

Equations 1.30 give a set of equations where the parallel and perpendicular component of the waves are independent. Solving that set with respect to each parallel/perpendicular component it is obtained:

$$\frac{R_\parallel}{A_\parallel} = \left[\frac{(1 - \delta_2)\sin\vartheta_i - (1 - \delta_1)\sin\vartheta_t}{(1 - \delta_2)\sin\vartheta_i} + (1 - \delta_1)\sin\vartheta_t\right] \tag{1.31a}$$

$$\frac{R_\perp}{A_\perp} = \left[\frac{(1 - \delta_1)\sin\vartheta_i - (1 - \delta_2)\sin\vartheta_t}{(1 - \delta_1)\sin\vartheta_i} + (1 - \delta_2)\sin\vartheta_t\right] \tag{1.31b}$$

$$\frac{T_\parallel}{A_\parallel} = \frac{2(1 - \delta_1)\sin\vartheta_i}{(1 - \delta_2)\sin\vartheta_i + (1 - \delta_1)\sin\vartheta_t} \tag{1.31c}$$

$$\frac{T_\perp}{A_\perp} = \frac{2(1 - \delta_1)\sin\vartheta_i}{(1 - \delta_1)\sin\vartheta_i + (1 - \delta_2)\sin\vartheta_t} \tag{1.31d}$$

Equations 1.31 are the **Fresnel formula** for reflection at a plane surface. Combining them with Equation 1.23 it is obtained:

$$\frac{R_\parallel}{A_\parallel} = \frac{(1-\delta_2)^2 \sin \vartheta_i - (1-\delta_1)\sqrt{(1-\delta_2)^2 - (1-\delta_1)^2 \cos^2 \vartheta_i}}{(1-\delta_2)^2 \sin \vartheta_i + (1-\delta_1)\sqrt{(1-\delta_2)^2 - (1-\delta_1)^2 \cos^2 \vartheta_i}} \tag{1.32a}$$

$$\frac{R_\perp}{A_\perp} = \frac{(1-\delta_1)^2 \sin \vartheta_i - \sqrt{(1-\delta_2)^2 - (1-\delta_1)^2 \cos^2 \vartheta_i}}{(1-\delta_1)^2 \sin \vartheta_i + \sqrt{(1-\delta_2)^2 - (1-\delta_1)^2 \cos^2 \vartheta_i}} \tag{1.32b}$$

$$\frac{T_\parallel}{A_\parallel} = \frac{2(1-\delta_1)(1-\delta_2) \sin \vartheta_i}{(1-\delta_2)^2 \sin \vartheta_i + (1-\delta_2)\sqrt{(1-\delta_2)^2 - (1-\delta_1)^2 \cos^2 \vartheta_i}} \tag{1.32c}$$

$$\frac{T_\perp}{A_\perp} = \frac{2(1-\delta_1) \sin \vartheta_i}{(1-\delta_1) \sin \vartheta_i + \sqrt{(1-\delta_2)^2 - (1-\delta_1)^2 \cos^2 \vartheta_i}} \tag{1.32d}$$

When ϑ_i is such that:

$$\cos \vartheta_c = \frac{1-\delta_2}{1-\delta_1} \tag{1.33}$$

that angle is named critical angle ϑ_c, and

$$\frac{R_\parallel}{A_\parallel} = \frac{R_\perp}{A_\perp} \tag{1.34}$$

this case correspond to a wave that is totally reflected. Normally the total external reflection take place at an interface light material(air/vacuum) and dense material, so $\delta_1 = 0, \delta_2 = \delta$, the equations became:

$$\cos \vartheta_c = 1 - \delta \qquad for \ small \ angle \qquad \vartheta_c \simeq \sqrt{2\delta} \tag{1.35}$$

and:

$$\frac{R_\parallel}{A_\parallel} = \frac{(1-\delta)^2 \sin \vartheta_i - \sqrt{(1-\delta)^2 - \cos^2 \vartheta_i}}{(1-\delta)^2 \sin \vartheta_i + \sqrt{(1-\delta_2)^2 - \cos^2 \vartheta_i}} \tag{1.36a}$$

$$\frac{R_\perp}{A_\perp} = \frac{\sin \vartheta_i - \sqrt{(1-\delta)^2 - (1-\cos^2 \vartheta_i}}{\sin \vartheta_i + \sqrt{(1-\delta)^2 - \cos^2 \vartheta_i}} \tag{1.36b}$$

$$\frac{T_\parallel}{A_\parallel} = \frac{2(1-\delta) \sin \vartheta_i}{(1-\delta)^2 \sin \vartheta_i + \sqrt{(1-\delta)^2 - (1-\cos^2 \vartheta_i}} \tag{1.36c}$$

$$\frac{T_\perp}{A_\perp} = \frac{2 \sin \vartheta_i}{\sin \vartheta_i + \sqrt{(1-\delta)^2 - \cos^2 \vartheta_i}} \tag{1.36d}$$

introducing the absorbing coefficient $\beta_2 = \beta \neq 0$:

$$\frac{R_\parallel}{A_\parallel} = \frac{\bar{n}^2 \sin \vartheta_i - \sqrt{\bar{n}^2 - \cos^2 \vartheta_i}}{\bar{n}^2 \sin \vartheta_i + \sqrt{\bar{n}^2 - \cos^2 \vartheta_i}} \tag{1.37a}$$

$$\frac{R_\perp}{A_\perp} = \frac{\sin \vartheta_i - \sqrt{\bar{n}^2 - \cos^2 \vartheta_i}}{(\sin \vartheta_i + \sqrt{\bar{n}^2 - \cos^2 \vartheta_i}} \tag{1.37b}$$

$$\frac{T_\parallel}{A_\parallel} = \frac{2\bar{n} \sin \vartheta_i}{\bar{n}^2 \sin \vartheta_i + \sqrt{\bar{n}^2 - \cos^2 \vartheta_i}} \tag{1.37c}$$

$$\frac{T_\perp}{A_\perp} = \frac{2 \sin \vartheta_i}{\sin \vartheta_i + \sqrt{\bar{n}^2 - \cos^2 \vartheta_i}} \tag{1.37d}$$

For interface that are curved, the Equations 1.37 are still valid if the curvature radius is much grater that the wavelength, condition that is satisfied for the X-ray radiation. The reflectivity are defined in this way:

$$R_p = \frac{R_\parallel}{A_\parallel} \left(\frac{R_\parallel}{A_\parallel} \right)^* \tag{1.38}$$

and

$$R_p = \frac{R_\parallel}{A_\parallel} \left(\frac{R_\parallel}{A_\parallel} \right)^* \tag{1.39}$$

Figure 1.4a, show the behaviour of an ideal non absorbing material ($\beta = 0$), where the reflection maintain its initial value up to the critical angle, and after fall down, in a way ruled by the dispersion coefficient δ which depend on the energy. In reality β is never zero, so it is not possible to have total external reflection in the way defined before. It is convenient to define that the total external appear when there is a point of inflection in the reflection curve with respect to the incidence angle ϑ_i, this occurs when:

$$\beta < 0.63\delta \tag{1.40}$$

In Figure 1.4 are plotted the reflectivity trend of three material (Si, Rh, Pb) with respect to the incidence angle, fixing the energy of the radiation at $5000eV$, on a silicon substrate. As it is figured there is a better behaviour, in sense of critical angle, for the light element because of them minor absorption coefficient β. This dependant mirror reflectivity is not implemented in my python library MONWES (but it could be done).

(a) Reflectivity for the case of a non-absorbing material

(b) Si

(c) Rh

(d) Pb
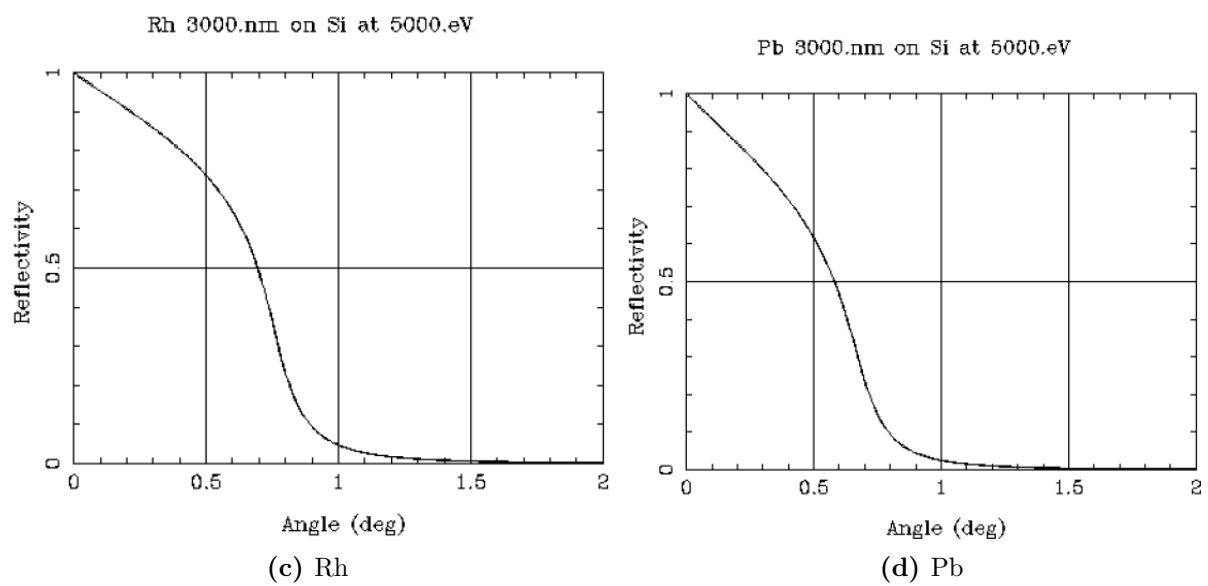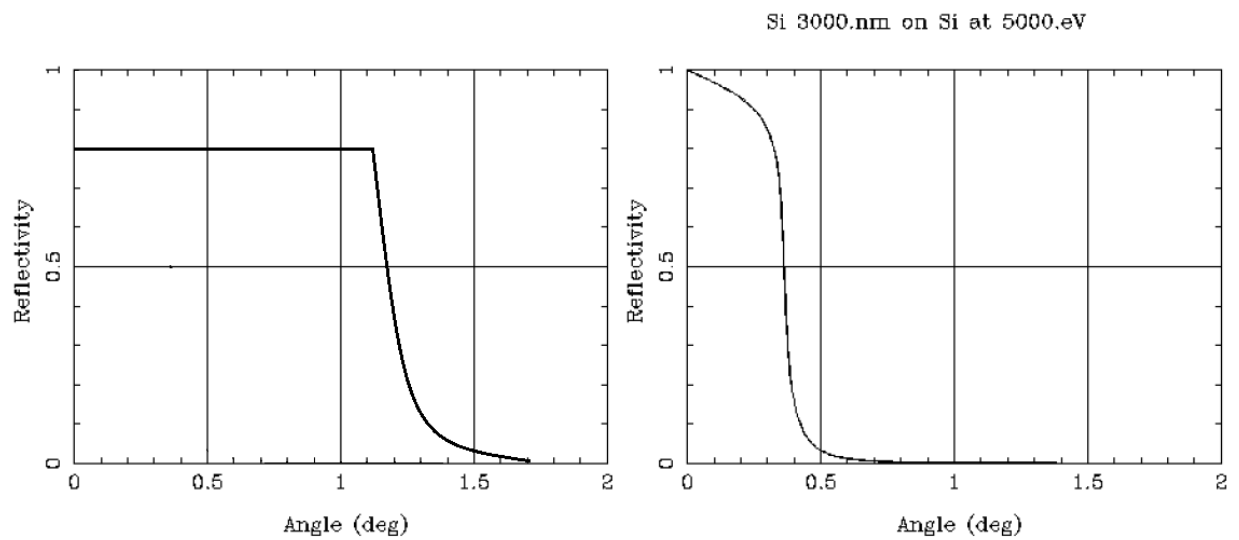
Figure 1.4: Reflectivity plot with respect of the grazing incidence angle ϑ_i of different material with a radiation of $500eV$ on a substrate of Si [LBN10]. It is also plotted the behaviour of an ideal non-absorbing material 1.4a

Chapter 2

Mirrors for X-rays

As discussed in Chapter 1, to focus X-ray radiation, refraction(compound refractive lenses) and reflection optics (curved mirrors) can be used. In this chapter the reflection optics is discussed because it is the main effect used in my python library. These optics are used in a grazing configuration because with small critical angle for total external reflection for X-ray radiation. The first part of this Chapter discuss as the focusing property of the simplest curved mirror, the spherical one, showing that it can't be used due to its intrinsic aberrations that are huge in a grazing incidence configuration. Then toroidal and conical mirror will be introduced, that cancel out some kind of aberration with respect to the spherical mirror. In the last part the concept of imaging system is discussed. Then two configurations of conical mirror used to focus the radiation in the synchrotron beamline are explained: the KirckPatrick-Baez system, very popular at ESRF, and the Montel system, that is the main object of my thesis.

2.1 Spherical surface

Mirrors that carry out any focusing must have a curved surface, is the spherical mirror, the simplest one, that it is defined only by one parameter, the radius of curvature. This mirror works well for normal incidence reflection, but, in a grazing configuration, it is affected by many kinds of aberrations. Here we discussed the:

1. astigmatism

2. spherical aberration

that are the main aberration that affect the X-ray radiation.

2.1.1 Astigmatism

"Rays that propagate in two perpendicular planes have different foci". This is the definition of astigmatism. In Figure 2.1 it is showed the image formation of a beam with a spherical mirror of radius R, at grazing incidence ϑ_i. Supposing that all the rays exiting from the source P are focused in the same point Q, and considering only the part of the beam that hit the portion of the mirror NO, it is
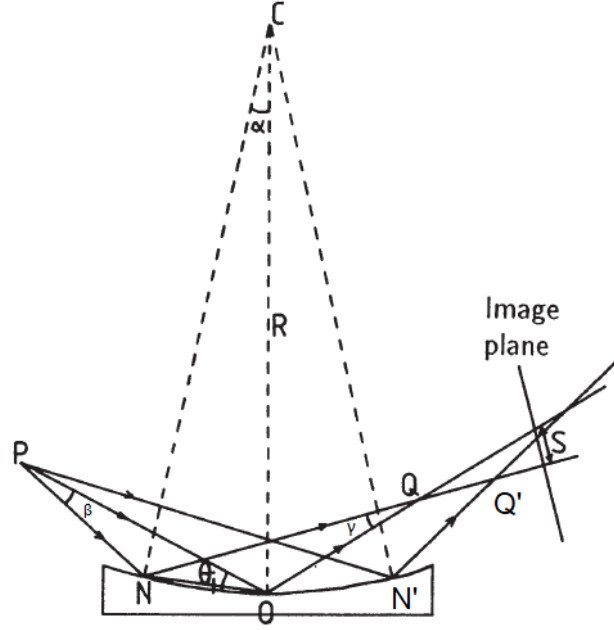
Figure 2.1: Formation image of a circular mirror for a point-wise source placed at a
distance PO from the center of the mirror. R is the curvature of the mirror,
ϑ_i the angle of the central ray.

possible to define β as the source divergence, γ the image divergence, u the distance
PO and v the distance OQ . The beam hit the mirror over a distance equal to
$k = $ NO, such as $k << R$, that correspond to a small divergence β. The cord
NO subtends an angle α with the center of the sphere C, thus $k = R\alpha$, γ is the
convergence angle of the beam at the focal point Q. For small angle approximation,
from the triangle PNO ,

$$\beta = R\alpha \frac{\vartheta_i - \alpha/2}{u - R\alpha} \tag{2.1}$$

and from QNO

$$\gamma = R\alpha \frac{\vartheta_i + \alpha/2}{v + R\alpha} \tag{2.2}$$

The reflection law impose that $\beta + \gamma = 2\alpha$, thus:

$$\frac{1 - \alpha/(2\vartheta_i)}{u - R\alpha} + \frac{1 + \alpha/(2\vartheta_i)}{v + R\alpha} = \frac{2}{R\vartheta_i} \tag{2.3}$$

in case of paraxial approximation

$$\frac{1}{u} + \frac{1}{v} = \frac{2}{R\vartheta_i} = \frac{1}{f_m} \tag{2.4}$$

where

$$f_m = \frac{R\vartheta_i}{2} \tag{2.5}$$

more generally

$$f_m = \frac{R sin\vartheta_i}{2} \tag{2.6}$$
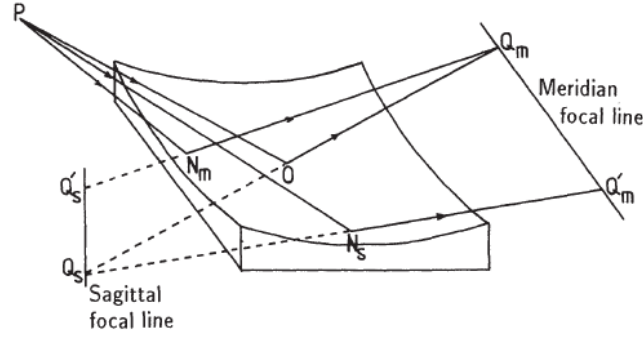
Figure 2.2: Image formation of a spherical mirror. The formation of a point wise source correspond to a two rods, one in the sagittal plane, and the second one in the meridian plane

f_m is named meridian focal length.
In case of a spherical mirror, a second image is generated in the sagittal plane, as it is showed if Figure 2.2, with a focal distance equal to:

$$f_s = \frac{R}{2 \sin \vartheta_i} \tag{2.7}$$

and it is named sagittal focal length. For Figure 2.2 it is possible to note that the two image for a point wise source are lines, where the meridian line is in the plane of the mirror and the sagittal line perpendicular to it. Equation 2.5 and Equation 2.7, are equal for incidence angle $\vartheta_i = 90°$, and correspond to have a stigmatic image (image without astigmatism). In the case of grazing incidence the situation is bad, for example, with a $\vartheta_i = 2°$, the sagittal focal length is 10^3 times the meridian length.

2.1.2   Spherical Aberration

Another aberration that affects a spherical mirror is the one named spherical aberration. Figure 2.1 shows that the rays are focused in different position, depending on the portion of the mirror that hit, for example the ray PN is focused in Q, and the ray PN' in Q'. This aberration can be determined relating it with the variation of v with α:

$$S = \Delta v \sin \gamma \simeq \Delta v \gamma \tag{2.8}$$

where S is the image size that determine the spherical aberration. Moreover, from Equation 2.3, in case of $\alpha = 0$:

$$v_0 = \frac{f_m u}{u - f} \tag{2.9}$$

otherwise:

$$v = v_0 + \Delta v = f_m u - \frac{\frac{3uR\alpha}{4} + \frac{R^2\alpha^2}{2}}{u - \frac{3R\alpha}{4} - f_m} \tag{2.10}$$

defining a magnification such as

$$M = \frac{v}{u} \tag{2.11}$$

combining it with Equation 2.1 and Equation 2.2

$$\gamma = \frac{2\alpha}{M+1} \qquad (2.12)$$

So

$$S = \frac{3R\alpha^2}{2}(M+1) = \frac{3k^2}{2R}(M+1) \qquad (2.13)$$

the dependence of S with respect to k is quadratic, so all the rays are deviated to the same side of $\alpha = 0$ image point.

2.1.3   Reducing aberrations

For spherical mirror it is possible to reduce the aberrations using large grazing angle (decrease astigmatism) and small aperture (decrease spherical aberration). The first solution is limited by the ϑ_c, for the total external reflection of the order of some milliradiant, for X-ray energies, that create a very huge astigmatism for spherical mirror. Reducing the aperture it means to reduce k but, this, affect the collecting power of the mirror reducing it. This is bad because the resolving power is limited by the diffraction limit that is $\simeq \frac{\lambda}{2\vartheta}$, where ϑ is the maximum semiaperture, that, for grazing angle, correspond to ϑ_i.
There is another way to reduce or cancel the aberration, using mirrors with different shape. If we want to reduce the astigmatism, toroidal mirrors are very useful, if we want to reduce spherical aberration ellipsoidal mirrors can be used used. These kind of aspherical mirror are reported in the following section.

2.2   Conic Surfaces

As it is said before, to go beyond the spherical mirror correcting the aberration, aspherical surfaces can be used. They are defined with more than one parameter, in general by an analytical formula. The easier aspherical surface is the toroidal surface, a surface that has two radii of curvature, the meridian one R_m and the sagittal one R_s. A particular choice of radii can be

$$R_s = R_m \sin^2 \vartheta_i \qquad (2.14)$$

in such a way to have equal focal length and so no astigmatism. Other kind of aspherical surfaces are those named "*conic surfaces*" that can be defined, approximately, as

$$z = \frac{cx^2}{1 + \sqrt{1 - (1+k)c^2 x^2}} \qquad (2.15)$$

where c is the base curvature at the vertex, k is a constant that define the kind of conical surface, and x is the radial coordinate of the point on the surface. In Table 2.1, and in Figure 2.3 is showed the relation between the k constant and the kind of surface
A good point that have the conical surfaces is the possible elimination of spherical aberration. As said in before, the spherical surface is affected by spherical aberration

Conic Constant k	Surface Type
0	Circle
$k < -1$	Hyperbola
$k = -1$	Parabola
$-1 < k < -0$	Ellipse
$k > 0$	Oblate Ellipse

Table 2.1: Parameter k of different conic surfaces
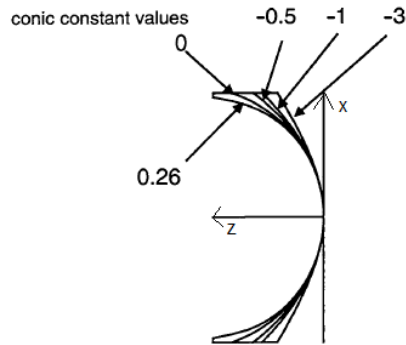
Figure 2.3: Different kind of surface conic, with the same c curvature value, and different constant k.

if the configuration is away from the normal incidence. The ellipsoidal geometry forms a point-to-point free-aberration focus where source and image are both real. On the contrary the hyperbola work for conjugates foci on different side of it. A parabolic surface creates a perfect image for any axial object place at infinity, this is the reason why parabolic mirror are very used for astronomical application. For all the shapes of surfaces, if the object is moved from its ideal position aberration will appear: an axial movement introduce a certain amount of spherical aberration, lateral movement introduce other types of aberration such as coma, astigmatism and field curvature.

Figure 2.4 show a simple example of how it is possible to correct the spherical aberration using a paraboloid mirror 2.4b instead of a spherical mirror 2.4a

(a) Spherical mirror **(b)** Parabolic Mirror
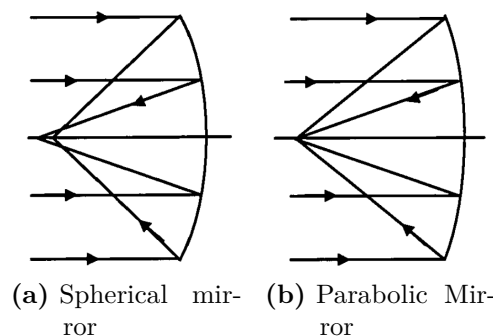
Figure 2.4: Example of spherical aberration correction
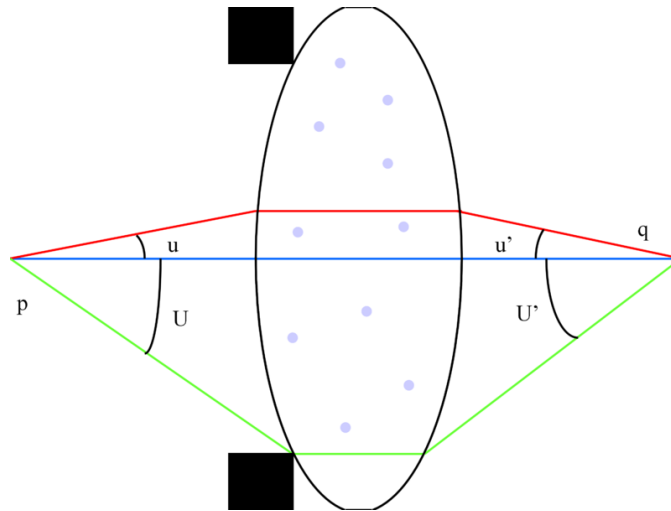
Figure 2.5: Sine Abbe condition for a lens

2.3   Compound Optical system

Simple mirror work well for a point-to-point optical system, but, to reproduce correctly an object image with the same aspect ratio it needed an imaging system. A system like this must satisfy the Sine-Abbe condition

$$\frac{sinu'}{sinU'} = \frac{sinu}{sinU} \tag{2.16}$$

where, as it is showed in Figure 2.5, u and u' are rays that leave the object, U and U' are the angles of the same rays that reach the image plane. In other words, the sine of the ray that leave the object must be proportional to the sine of the angles that reach the image plane. Unfortunately, for the case of mirror, there is no way to satisfy the Sine Abbe condition using only one mirror. To satisfy the condition, and so obtain a better image, there are optical systems composed by more than one mirror. One is the Wolter system, widely used in astronomy, that use a combination of coaxial and confocal conic section. A first approximation system that respects the sine Abbe condition are the Kirkpatrick-Baez and Montel system. These systems are compound optical systems involving meridian focusing at right angle planes.

2.3.1   Wolter System

In 1952 Wolter published a paper [Wol75] in which he discussed several dispositions of two conical mirrors in order to collect light for an astronomical use. Figure 2.6 show the different type op systems: Wolter I, Wolter II, Wolter III.Wolter I telescope consist of a coaxial paraboloid (primary mirror) and hyperboloid (secondary mirror). The focus of the paraboloid is coincident with the rear focus of the hyperboloid, and the reflection inside both mirrors. The Wolter II telescope use the same kind of mirror of Wolter I paraboloid and hyperboloid. But the focus of the paraboloid coincident with the front focus of the hyperboloid, and, the reflection, occurs internally for the paraboloid and externally for the hyperboloid.

(a) Wolter I

(b) Wolter II
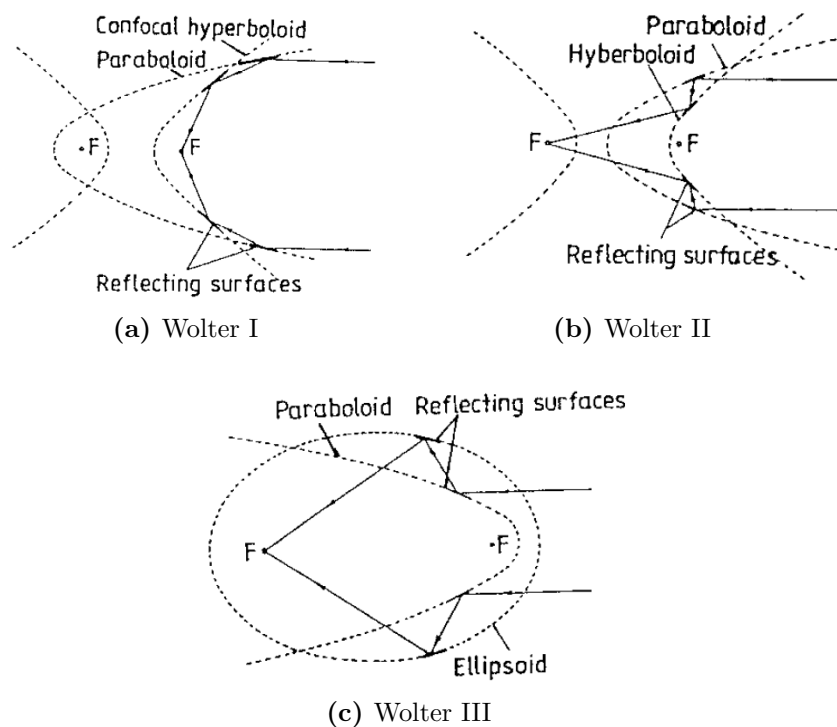
(c) Wolter III

Figure 2.6: Different kind of Wolter System [SS05]

The Wolter III telescope consist in a paraboloid and an ellipse. In this system the first mirror is the paraboloid one, and the second is the ellipsoidal that have front focus coincident with that of the parabola, moreover the reflection is external for the paraboloid and internal for the ellipsoidal. The Wolter I have typical grazing angle of less than a degree and is used for hard X-rays. The Wolter II telescope has typical grazing angle of, approximate, 10 degree and is used for soft X rays and extreme ultraviolet (EUV). Because of circular symmetry, astigmatism and spherical aberration are eliminated but exhibit coma aberration. Other problem is the difficulty of fabrication , and require a huge area to achieve a very small collecting angle.

2.3.2 Kirkpatrick-Baez System

In 1948, Kirkpatrick and Baez proposed ([KB48]) an X-ray focusing optical system consisting of two total reflection elliptical mirrors, which aligned perpendicularly (Figure 2.7). This focusing optical system is very popular at the ESRF due to its potential to remarkably improve the performance characteristics of X-ray by enabling more efficient collecting of X-rays than in other methods. A further advantage is that the method maintains the focusing state with the same optical arrangement even if the wavelength of the X-rays is shifted. However, to realize X-ray beams with an ideal focal size, high efficiency and absence of background noise around a main peak, it is necessary to prepare elliptical mirrors having a very high quality. Since the two mirrors are not coincident, the object distance for the meridian reflection in the first mirror is less than that for the

sagittal reflection in the second mirror. Thus, the magnification is different in the two directions.

Figure 2.7: Kirkpatrick-Baez system

2.4 Montel

Another possibility to dispose mirrors creating a focalizing or colimating optical system consist in the disposition of two orthogonal mirrors attached one to the other as showed in Figure 2.8. This geometry is called Nested Kirkpatrick-Baez system or Montel system [Mon57]. To go beyond current state-of-ar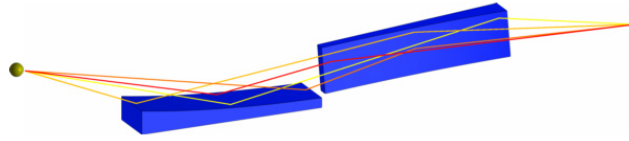t performances, new approaches are required that can collect more divergence than with standard sequential Kirkpatrick-Baez (KB) X-ray mirrors. Indeed, the quality of x-ray mirrors has now reached the diffraction limit, and simply more perfect KB mirrors cannot decrease spot size because of different magnification in horizontal and vertical.
In this section we first describe of the Montel system with its advantages and disadvantages with respect to the KB system. Then there is an explanation on the optical design method.

2.4.1 Description

Because of its distinctive design, Montel system have numerous advantages over traditional Kirkpatrick–Baez system. In contrast to KB systems where the two reflective surfaces are arranged in-line one after the other, those in Montel optics are mounted side by side at 90 to each other (Figure 2.8). Due to this fact, the incident X-ray beam now undergoes reflection simultaneously from both surfaces instead of being reflected sequentially as in the KB system. Hence, the mirror-focal point distance is diminished and consequently the demagnification ratio increased. The gain can be substantial especially when the focal distance is comparable with the mirror lengths. Furthermore, the side-by-side geometry offers a more compact design and therefore represents a convenient solution when space availabilities for optical elements are highly restrictive. In terms of mechanical structures, KB optics usually require two independent sets of alignment stages for each mirror. It is possible, in the Montel system, to assemble both surfaces together with their stages onto a common platform. Apart from providing a compact solution, this can also help in reducing the sources of parasitic vibrations as well as any individual misalignment between the mirrors. Lastly, since in this geometry that want to the second mirror is positioned closer to the source than in the KB system, for the same angular acceptance in both mirror systems, a shorter mirror is needed in the Montel optics design. This is highly desirable as significantly better figure errors can be achieved for smaller mirror sizes than larger ones with the overall benefit of yielding less aberrated beams.
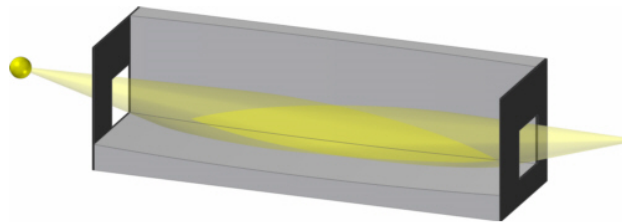
Figure 2.8: Montel system

However Montel configuration, presents some draw-back with respect to the sequential KB system. The fact that the beam hit the worst part of the mirrors, the edge, that are less polished thus contain more surface defect, decreases the quality of the reflection.

2.4.2 Optical Design [IBK09]

The mirrors used in this Montel configuration are mirror that have a plane shape in one direction and elliptical shape in the other direction. They are cylinders of elliptical section. One approach to obtain the Montel system is that to use two pre-figured elliptical mirrors and grind the cut side at 45° as shown in Figure **??**. Then the mirrors are placed together making a good fit with no gap requiring no contouring of the mirror side. Another way involves dividing pre-figured elliptical mirror into two parts that are added together, forming the Montel system. These approaches are primary driven by the fact that in a conventionally polished mirror the clear aperture area has the best figure and finish. As such, using two halves of a prefigured mirror cut in the middle has several advantages- including consistency and economy. There are major challenges however. First, the mirror surface must be protected against damage and deformation during cutting and subsequent figuring operations. After cutting into two, the cut sites must be treated (e.g., etched) to remove any subsurface damages that could alter a mirror's figure. Then the mating side of one of the mirrors must be contoured and polished such that when it is placed against the partner mirror, it makes a nearly perfect fit with good surface quality all the way to the contact edge This last two-steps are crucial because if there is a significant gap or if the mirror surfaces in the vicinity of the interface are damaged, a significant part of the incident beam could be lost. As an example, are developed a pair of Montel mirrors for poly-chromatic nano focusing on Sector 33 at APS. This beam line will use 40 mm long elliptical mirrors for nano-focusing a 100 μm beam to a 50 nm spot at 2000x demagnification. This concave elliptical mirror has a maximum depression of about 6 μm at its centre. If cut flat and placed against its mating mirror, a gap as large as 6 μm is created which loses about 10% of the 100 μm incident beam. Similarly, if the mirror surfaces near the intersection are damaged, then beam loss can be significant.
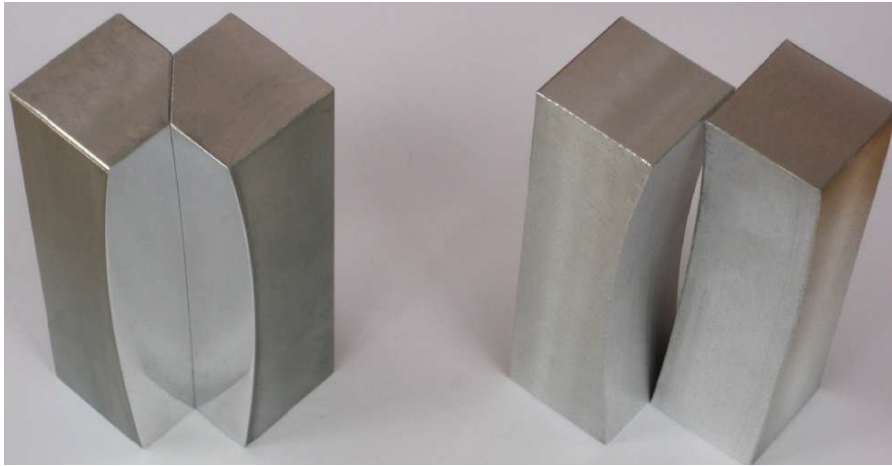
Figure 2.9: Example of how a Montel system is built from two cylindrical mirrors cutting the edge with at angle of 45°.

Chapter 3

MONWES

Chapter 3 goes deep in the description of the python library developed by me. MONWES (MOntel and Wolter of yunES) library is a python library that perform ray tracing simulations for x-ray radiation along a system consisting of one or several mirrors, using the optical element and compound optical elements introduced in Chapter 2. The library take inspiration from OASYS ray tracing software developed by Manuel Sanchez Del Rio of ESRF, taking the starting element already present in OASYS environment in order to have the basic element that will be used in the new Montel system. OASYS elements are written for a sequential tracing method, method that doesn't work for Montel system. Thus a great effort has been done to generate a new tracing system that use a parallel approach.

Object oriented programming were used consisting in a programming method in which data structures are defined with their type of operation, that are applied to the data structure. This oriented programming is based on the concept of "objects", it contains data in form of fields known as attributes and code in the form of procedure known as methods [GHJV95].

The final goal of the MONWES library is that to complement the standard ray tracing code SHADOW in OASYS with compound elements.

The library and also this Chapter, is composed by three main elements:

1. Beam object: containing the information of the beam along the beamline;

2. Optical element: that initialize the characteristic of the optical element/system used in the beamline;

3. Tracing system: that relates the Beam characteristic with the effect of the optical elements/systems.

3.1   Beam

Beam object is the object that contain the spatial and velocity information of a collection of rays. The Beam object is mainly characterized by four parameters:

- Number of rays

- Spatial profile

- Divergence profile

- Flag vector

Having a large number of rays is useful in terms of results but increase the computation time, so, one has to find a compromise between the number of rays and the computation time depending on the quality desired. By default, the number of rays, is set $25 * 10^3$ that allow to have good results without spending lot of time. Figure 3.1 show an initialization of Beam setting the number of ray equal to 10^4.

```
1    from monwes.Beam import Beam
2
3    beam = Beam(N=10**4)
```

Figure 3.1: Example of Beam initialization

The Beam is initialized with its number of rays and the spatial and divergence profile. For the spatial profile there are some possibilities that correspond to different geometrical figure such as: rectangular profile, circular profile, Gaussian profile, point wise profile. The default one is the point wise profile, that it is useful for ideal testing, in this case, there is no input parameter are needed. All the other profiles are parametrized by external input that depends on the nature of the profile. For the Gaussian profile the parameter needed is the σ_x and σ_z that correspond the σ of the two dimension, Figure 3.2a shows a code example to define a Gaussian spot of a Beam having $25 * 10^3$rays with the two σ different, $\sigma_x = 0.1mrad, \sigma_z = 1mrad$ as it is showed in Figure 3.2b.

```
1    from monwes.Beam import Beam
2
3    beam = Beam()
4    beam.set_gaussian_spot(1e-4, 1e-3)
```


(a) Example code for a Gaussian source in spatial coordinate
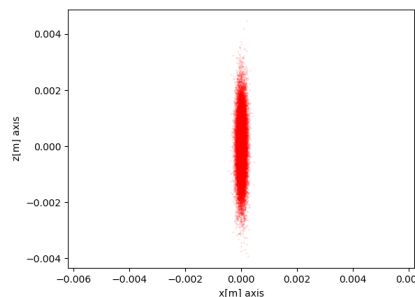
(b) Plot of Figure 3.2a

Figure 3.2: Example 1

Over the Gaussian profile, there are other two geometrical profile that can be defined: rectangular and circular. They have a uniform distribution of rays in their space domain. For the rectangular distribution the parameter to define are the xz limit of the coordinate that define the sides of the rectangle. Figure 3.3a shows an example code where it is defined a circular profile with a radius of 1cm and, after,

it is overwritten by another geometrical profile having a rectangular shape. In this case the final profile of the Beam is shown in Figure 3.3b.

(a) Example code for a circular and a rectangular spot

(b) Example plot of the rectangular profile
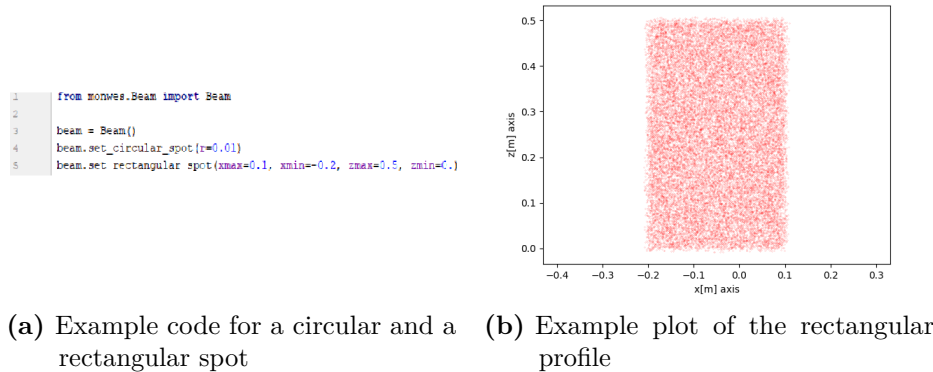
Figure 3.3: Example 2

It is possible to define a special shape that have, more or less, the figure of a person with a uniform distribution of the point in all the point of the space. This special shape is showed in Figure 3.4a, that is defined in the code written in Figure 3.4b. It is used to do a test "imaging" of a system checking that the image, after the optical system, is affected by deformation or defect. As it is showed, the "*initialize_ as_ person*" command take two input parameters, the number of the total rays (by default are $25 * 10^3$), and a size parameter that set the coordinate limit of the figure, more precisely. In Figure 3.4a the size correspond to 10^{-6} so the limit are: $x_{max} = 1\mu m$, $x_{min} = -1\mu m$, $z_{max} = 1\mu m$, $z_{min} = -20\mu m$.

(a) Example plot "person" profile

(b) Example code for the "person" spot
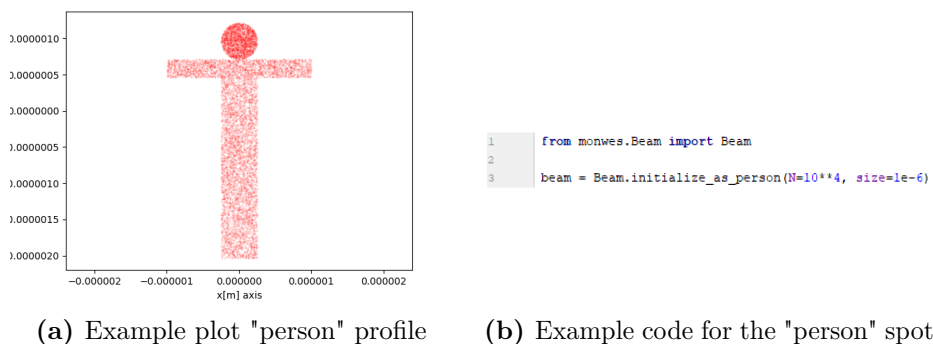
Figure 3.4: Example 3

The last piece of the Beam object is the "Flag" vector. Every component of this vector have a correspondence with a certain ray and contain the information about the number of optical element that, the ray, travel until a particular moment. Moreover, this value become negative when the ray doesn't hit an optical element, in such a way to have an information where the rays were lost. Figure 3.5, resume the main parameter of the Beam object with their default values

```
8       class Beam(object):

9

10          def __init__(self,N=25000):

11

12              N = round(N)

13

14              self.x = np.zeros(N)
15              self.y = np.zeros(N)
16              self.z = np.zeros(N)

17

18              self.vx = np.ones(N) * 0.
19              self.vy = np.ones(N) * 1.
20              self.vz = np.ones(N) * 1.

21

22              self.flag = np.zeros(N)

23

24              self.N = N
```

Figure 3.5: Summary of the Beam object parameter

A part from the principal characteristic treated above, Beam object contain methods or functions in order to manage better the information that it contain. The other option defined are reported here below:

- "*import_ from_*" file(filename='filename'): define a Beam with a characteristic defined in a file '.h5'

- "*set_ point*(x, y, z)": move the Beam in a part of the space centred in the coordinate (x,y,z)

- "*initialize_ from_ arrays*$(x, y, z, vx, vy, vz, flag)$": define a Beam with the spatial value defined in the array x,y,z, the velocities' value defined in the array vx,vy,vz and the flag value defined in the array flag

- "*duplicate*()": duplicate a Beam

- "*good_beam*()": define a Beam that, starting from another Beam, extract only the good rays (those that have a positive flag)

- "*part_ of_ beam*$(indices)$": define a Beam that, starting from another Beam, extract the ray that correspond to the position defined in the array indices

- "*number_ of_ good_ rays*()": return the values of the good rays

- "*merge*$(beam2)$": merge a beam1 with another beam2, the first part of this new beam correspond to the beam1, and the second part to the beam2

- "*retrace*$(distance)$": this correspond to a free propagation in the space of the Beam within a distance equal to "distance"

At the end there are the command that plot the various characteristic of the beam, that contain the information for the plotted characteristic, for example plot_ xy() make a plot of the x and y coordinate of the beam, plot_ good_ xpzp() make a plot of the x-velocities and z-velocities of only the rays that have a positive flag

3.2   Optical Elements

Because, as discussed in Chapter 1, mirrors are the principal elements used in synchrotron we first develop mirrors in the library. It is also interesting to implement an ideal lens that is useful to verify ideal focusing of the Beam. Only one kind of lens is implemented: ideal lens.

3.2.1   Mirrors

The different kind of mirror that are defined are:

- plane mirror

- spherical mirror

- ellipsoidal mirror

- paraboloidal mirror

- hyperboloidal mirror

All those geometrical shape are a subset of a surface conical figure. As is discussed in Chapter 2, and reported in Equation 3.1, a surface conic is defined by a series of coefficient.

$$a_0 x^2 + a_1 y^2 + a_2 z^2 + a_3 xy + a_4 yz + a_5 xz + a_6 x + a_7 y + a_8 z + a_9 = 0 \qquad (3.1)$$

The parameter needed to define the correct surface conic shape that define uniquely the mirror desired are:

- focal distances

- angle of incidence ϑ_g, more precisely the program use the complementary angle of ϑ_g that is $\vartheta = \frac{\pi}{2} - \vartheta_g$ (the input and output angle are in radiant)

The conic surfaces are defined in such a way to have the origin equal to the incidence point of a collimated ray distant p (that correspond to the object focal distance) from the mirror, and with the normal of the surface corresponding to the z-axis, as it is showed in Figure 3.8. For the plane mirror the situation is simple, because the equation of the surface is that in Equation 3.2, that have all the coefficient equal to 0 apart from a_8 that is equal to 1.

$$z = 0 \qquad (3.2)$$

For the spherical case, the parameter that characterize a sphere is the radius, one time defined the radius, the equation of the sphere is:

$$x^2 + y^2 + z^2 = r^2 \qquad (3.3)$$

Moreover, it is known, from the spherical lens optics (see Chapter 2) , that:

$$\frac{1}{p} + \frac{1}{q} = \frac{2}{r_t \sin \vartheta_g} \tag{3.4}$$

and

$$\frac{1}{p} + \frac{1}{q} = \frac{2 \sin \vartheta_g}{r_s} \tag{3.5}$$

where r_t, is the tangential radius, and r_s is the saggital radius. The sphere case has $r_t = r_s$, this mean that, apart from the normal incidence case, the sphere cannot perfectly focalize/collimate a beam. The radius chosen in "$Surface\_\ conic$" object is that corresponding to the equation 3.4:

$$r = \frac{2}{\sin \vartheta_g} \frac{pq}{p + q} \tag{3.6}$$

where p correspond to the object focus length, q to the image lengths, ϑ_g to the incidence angle.

For the paraboloid shape the correct coefficients that define the right surface are: the incidence angle, the focal distance and another parameter that distinguish between the cases shown in Figure 3.6a and, Figure 3.6b. These two system correspond mirrors that, physically, have different behaviour, the first one Figure 3.6a, focalize a Beam, the second one, Figure 3.6b, collimate a Beam.

(a) Focalizing case   **(b)** Collimating case
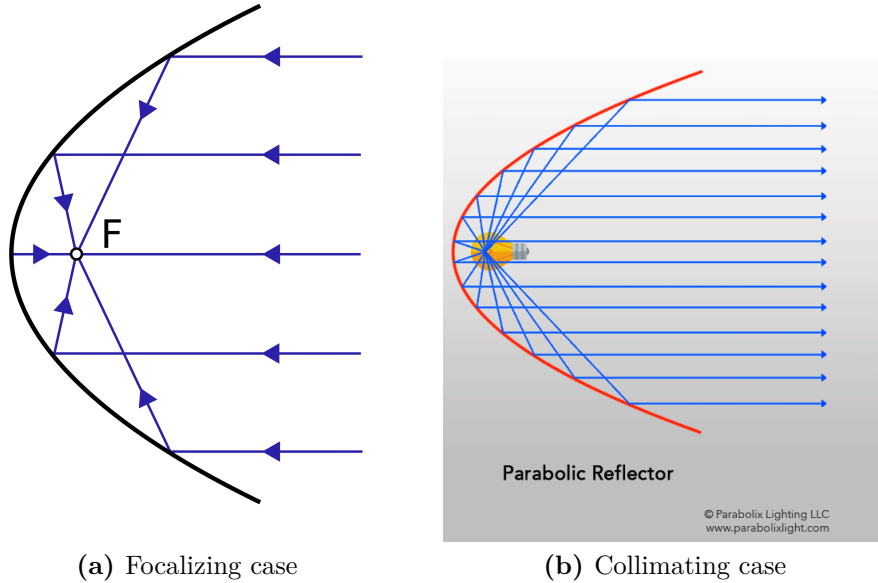
Figure 3.6: Parabola

The general equation of a parabola, such that in Figure 3.7 is

$$y = \frac{1}{4f} x^2 \tag{3.7}$$

where f is the focal distance of the parabola. After a few calculation, see Appendix A, it is possible to correlate f with the input parameter:

$$f = d \sin^2 \vartheta \tag{3.8}$$

where d is the object focal distance, in the case depicted in Figure 3.6a, otherwise, in the case depicted in Figure 3.6b, d is the image focal distance.
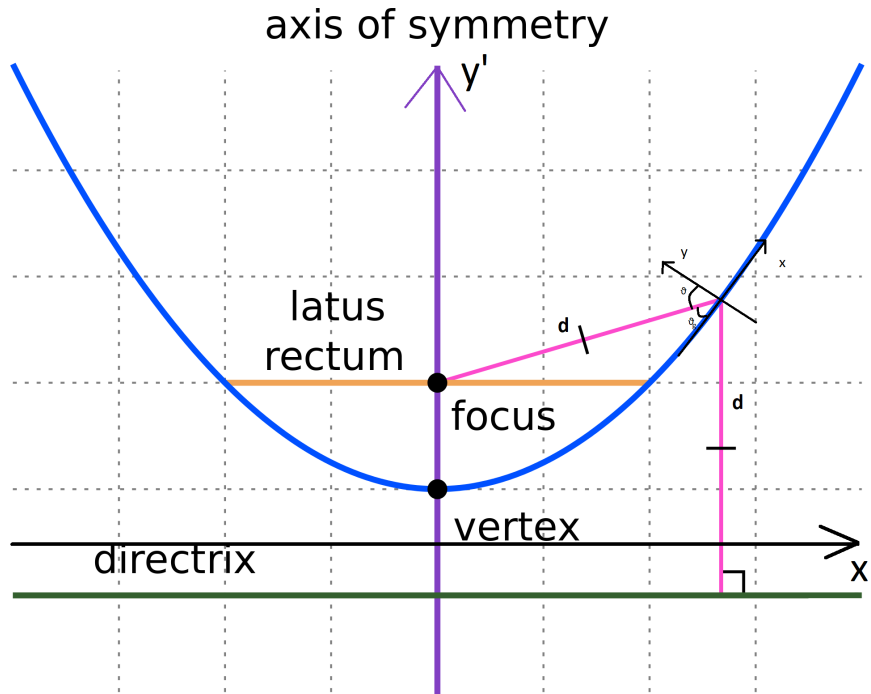
Figure 3.7: Part of a parabola (blue), with other characteristic (different color) [Wik18]

For the elliptical case the situation is represented in Figure 3.8. The general equation of an ellipse where appear two unknown a and b.

$$\frac{x^2}{a^2} + \frac{y^2}{b^2} = 1 \tag{3.9}$$

It is possible to correlate (Appendix A), the focal distances plus the incidence angle with the two parameter a and b with the following two equations:

$$p = \frac{a+b}{2} \tag{3.10}$$

$$q = \sqrt{ab}\cos\vartheta \tag{3.11}$$
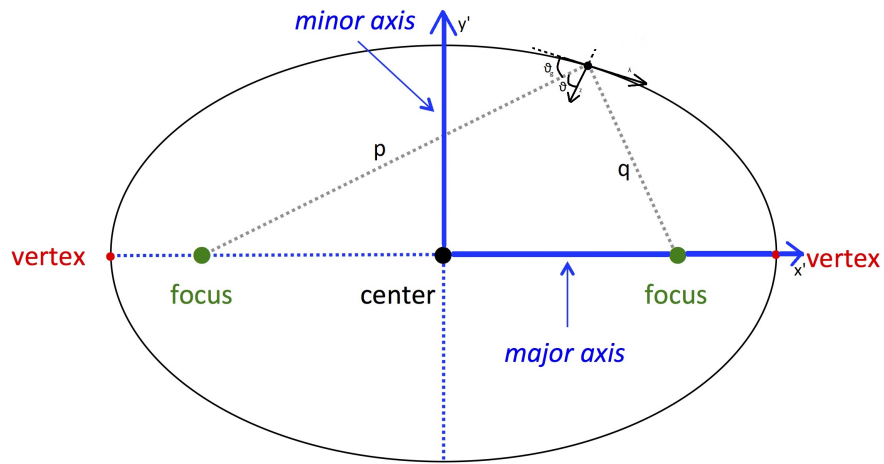
Figure 3.8: Ellipse System

Once the surface is defined in the $x'y'$ reference frame, thean it is done a rotation and a translation in order to center it in the new xy system centered on the point P. Normal at point P is the new z-axis.

For the hyperboloidal mirror the situation is similar to that of the ellipsoidal case, in fact, the general equation of the an hyperbola such the one in Figure is

$$\frac{x^2}{a^2} - \frac{y^2}{b^2} = 1 \tag{3.12}$$

and the equations that correlate the focal distances and the incidence angle with the parameter a and b are

$$p = \frac{a-b}{2} \tag{3.13}$$

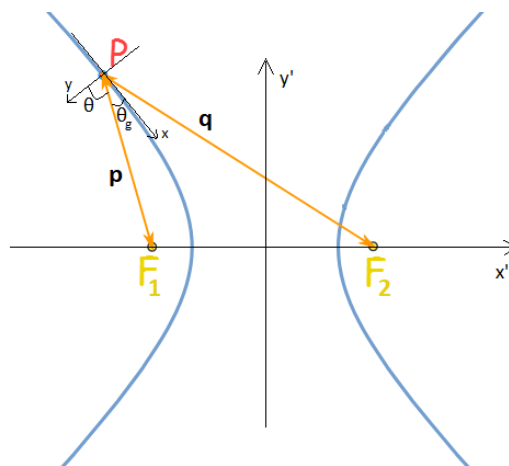$$q = \sqrt{ab}\sin\vartheta \tag{3.14}$$

Figure 3.9: Hyperbola System

After that, as in the case of the ellipsoidal mirror, a rotation and a translation is needed to complete the work.

In the program there is a further option that make the mirror cylindrical in one dimension maintaining its surface conic in the other. To do this, in "$Surface\_ conicobject$", it is defined a "$set\_ cylindrical$" method, that change the shape of the surface, from a complete revolution conic, to a surface conic in one dimension and cylindrical in the other.

In addition of the mirrors elements is implemented also an ideal lens element that follow the typical lens equation:

$$\frac{1}{f_x} = \frac{1}{p} + \frac{1}{q} \tag{3.15}$$

$$\frac{1}{f_z} = \frac{1}{p} + \frac{1}{q} \tag{3.16}$$

where f_x is the x focal length and f_z is the z focal length. For this optical element the input parameters are the object focal distance, image object distance and the two focal distances (f_x, f_z) that, in the default mode, are set equal with a value equal to $f_x = f_z = \frac{pq}{p+q}$.

3.2.2 Compound Optical Element (KB and Montel system)

This program include also two different system composed by more mirrors. Starting from conical mirrors, combining them, is possible to have a compound optical element that can simulate the behaviour of some typical instrumentation that characterize the facilities, in particular in the synchrotron world. The compound optical system implemented are two of those mentioned in Chapter 2

- Kirkpatrick-Baez system (KB system)

- Montel

3.2.3 Compound System: Kirkpatrick-Baez

KirkpatrickBaez or, more simply, KB system is shown in Figure 3.10. It is composed by two cylindrical conic mirrors placed one after the other with the two focal lengths that converge in the same point. There are implemented two different kinds of KB system, a first one composed by two elliptical mirrors and a second one composed by parabolic mirrors. The input parameters that the program needs are the two incidence angles and the two foci, with respect to the centre of the KB system, represented in Figure 3.11 and the separation of the two mirror, from centre to centre.
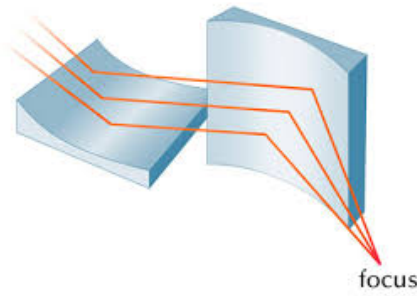
Figure 3.10: KB system
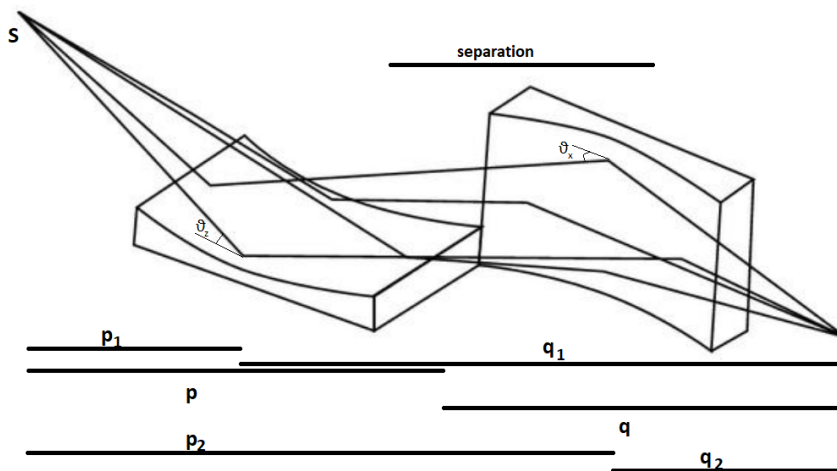
Figure 3.11: Different object/image focal length that characterize the whole KB system, and the single mirrors. Is it also showed the separation length between the two mirror

This system is simply a system composed by two conical mirrors in series. The parameter needed to define the mirror are not the ones defined by the user. The mirror parameters are the ones shown in Figure 3.11: p1, q1, p2, q2. These parameters represent the object focal distance (p1, p2) and the image focal distances (q1, q2) of the two mirror, as represented in Figure 3.11. Figure 3.12, show an example of the definition for a KB system that have an object focal length of 2m, an image focal distance of 5m, a separation between the two centre of the mirrors of 1m, and the two angle of incidence equal each other to 2°.

```python
from monwes.CompoundOpticalElement import CompoundOpticalElement
import numpy as np

theta = 88. * np.pi / 180
KB = CompoundOpticalElement.initialize_as_kirkpatrick_baez(p=2., q=5., separation=1., theta_z= theta)
```

Figure 3.12: Example 4

3.2.4 Compound System: Montel

The Montel system, depicted in Figure 3.13, is composed, as for the KB, by two surface conical mirror cylindrical in one direction, but, because the two mirror are not in series, as for the case of the KB, the situation is a bit complicate. Starting from definition of the two mirrors one is rotated of 90°, in order to have a mirror in the xy plane, and another one in the zy plane. As shown in Figure 3.13 the centre of the Cartesian system is set in the point where the optical axis of the system hit the compound system having the normal of the first normal equal to the z-axis, and the second normal equal to the - x-axis. The system is defined by the following parameters p, q, ϑ_z, ϑ_x, where p and q are the focal distances of the two mirrors and ϑ_z and ϑ_x are the angle of incidence to define the correct mirrors (by default $\vartheta_z = \vartheta_x$).
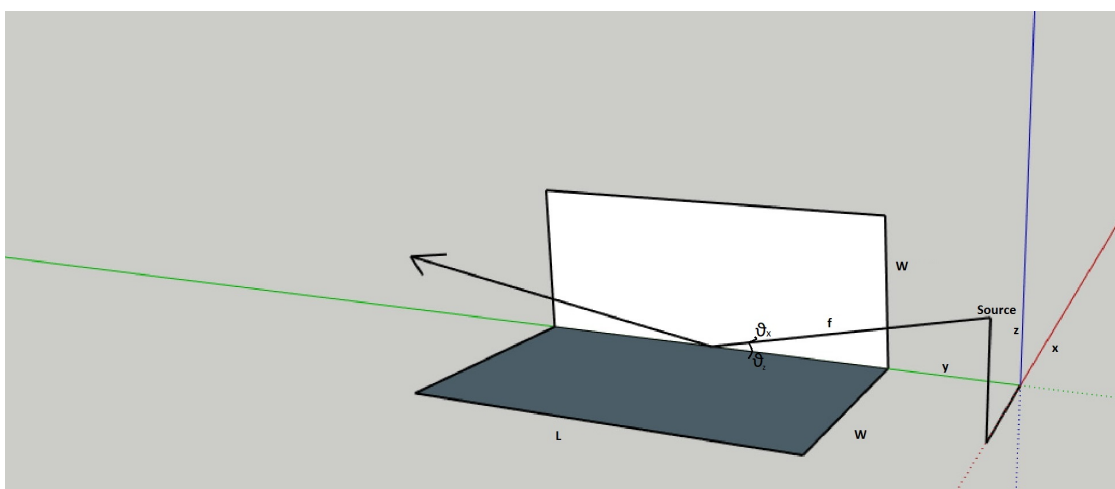

Figure 3.13: Grafical 3D view of the Montel in its reference system

The Figure 3.14 shows an example code for a parabolic Montel system having an object focal length of 5m, image focal length of 2m and the two incidence angle of 1.5°, that focalize a Beam. As for the KB system also in this case there are implemented two possibilities, an ellipsoidal system (having the two mirror as ellipsoid), and parabolic system (having the two mirror as ellipsoid).

```
1   from monwes.CompoundOpticalElement import CompoundOpticalElement
2   import numpy as np
3
4   theta = 88.5 * np.pi / 180
5   montel = CompoundOpticalElement.initialize_as_montel_parabolic(p=5., q=2., theta_z=theta, infinity_location='p')
```

Figure 3.14: Example 5

3.3 The tracing mechanism

Once defined the Beam and the different optical element, to complete a simulation, is needed a tool that put everything together and modify the property of the beam after the interaction with the optical elements.
For example, if one want to simulate the system depicted in Figure 3.15, one has to

define a Beam source, the optical element and, at the end the distances between the optical elements. The tracing part of the program, for the non-compound optical element, is written in such a way that the trace work in series, one optical element after the other. This works with the definition of two distances, object/image distance from the centre of the optical element, the incidence angle of the Beam. One possibility, to define the system in Figure 3.15 is to set the object distances of the mirrors equal to distance d_0 and d_1, and the image distances equal to 0, for the lens lets set the object distance equal to d_3 and the image distance equal to d_4 as it is reported in Figure 3.16.
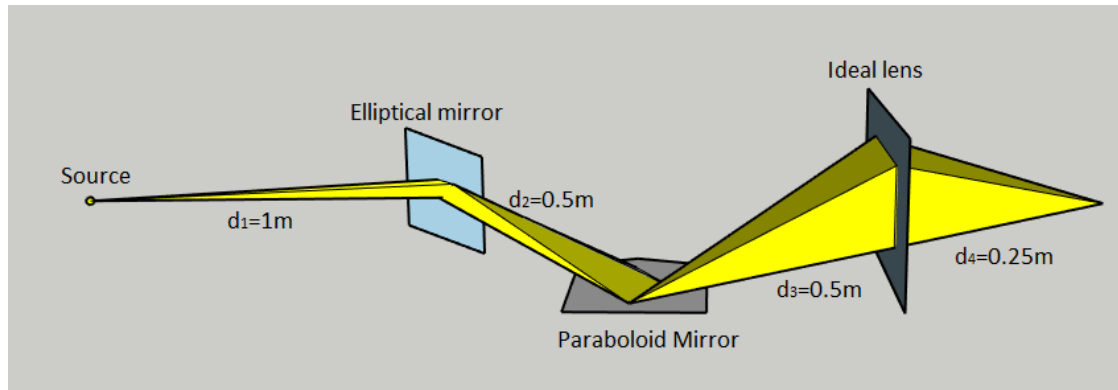

Figure 3.15: To simulate this system it need to define: source Beam parameters, optical elements and the distances between them

```
1    import ...
5
6
7    theta_e = 88.5 * np.pi / 180
8    theta_p = 88. * np.pi / 180
9    beam = Beam()
10   beam.set_gaussian_divergence(1e-3, 1e-4)
11
12   ell = Optical_element.initialize_as_surface_conic_ellipsoid_from_focal_distances(p=1., q=2., theta=theta_e)
13   par = Optical_element.initialize_as_surface_conic_paraboloid_from_focal_distances(p=0.5, q=2., theta=theta_p, infinity_location='p')
14   lens = Optical_element.initialiaze_as_ideal_lens(p=1., q=2.)
15
16   beam = ell.trace_optical_element(beam, p=1., q=0)
17   beam = par.trace_optical_element(beam, p=0.5, q=0., alpha=np.pi/180)
18   beam = lens.trace_optical_element(beam,p=0.5, q=0.25)
```

Figure 3.16: Example 6

3.3.1 Tracing for simple Optical element

Going deeper in the code, the algorithm that trace a single element is divided in 5 steps:

1. change the reference system from that of the optical axes to that of the optical element using two rotations, one along x-axis, and second along y-axis. Then a translation equal to the object distance of the optical element

2. free propagation up to the optical element

3. effect of the optical element (specular reflection)

4. free propagation to the image plane

5. changing the reference system to one that has the optical axis equal to the y-axis

The first three points are condensed in the method "*effect_ of_ the_ optical_ element*", that is showed in Figure 3.17a, and the last two point are condensed in the method "*effect_ of_ the_ screen*" that is showed in Figure 3.17b.

```
227    def effect_of_optical_element(self,beam):
228
229        self.rotation_to_the_optical_element(beam)
230        self.translation_to_the_optical_element(beam)
231        [beam, t]=self.intersection_with_optical_element(beam)
232        self.output_direction_from_optical_element(beam)
```

```
235    def effect_of_the_screen(self,beam):
236
237        self.rotation_to_the_screen(beam)
238        self.translation_to_the_screen(beam)
239        if np.abs(self.q) > 1e-13:
240            self.intersection_with_the_screen(beam)
```

(a) Example code for a Gaussian spot   **(b)** Plot of Figure 3.2a

Figure 3.17: Example 7

Because of the different definition, the tracing method of the rays' beam, need a different interpreter that can link the beam with the different optical elements that meet on his way. Because of the different nature, there are implemented two kinds of tracing, a first one that trace the KB system, that is composed by a series of optical elements and so can be used for all the compound optical elements that are in series. And a second one that is specific to the Montel system, because it is not composed by mirrors in series rather than mirrors in parallel, having the two elements in a very small region of the space that have in which order the rays of the beam hit the different mirrors.

3.3.2 Tracing for KB

For KB system the situation is more or less the same as for a simple optical mirrors, with the only difference that there are more than one mirror. So the algorithm to simulate the tracing system is nothing else than a for loop, that use the tracing system of the simple optical element. In this the object and the image distance from the centre of the system are the default ones, such as for the incidence angles. Figure 3.18, show the trace code for the compound elements that are in series.

```
372        def trace_compound(self,beaml):
373
374            beam=beaml.duplicate()
375
376            self.system_initialization(beam)
377
378            for i in range (self.oe_number()):
379
380                if self.oe[i] is not None:
381
382                    self.oe[i].effect_of_optical_element(beam)
383                    self.compound_specification_after_oe(i=i)
384                    self.oe[i].effect_of_the_screen(beam)
385                    self.compound_specification_after_screen(beam = beam, i=i)
386
387            return beam
```

Figure 3.18: Tracing code for a compound optical element that use a sequential tracing method, such as KB system.

3.3.3   Tracing for Montel

As it is said at the beginning of the Chapter, the tracing method used for Montel is new and different from the other. For the KB case the tracing method utilized is sequential. This mean that all the rays hit firstly a mirror, and secondly the other mirror. Figure 3.19, show the KB and Montel and situations respectively.
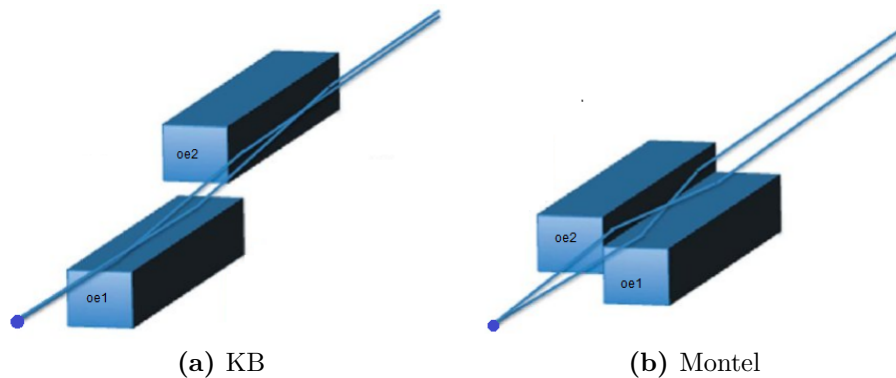

(a) KB   (b) Montel

Figure 3.19: For the KB system (3.19a) all the rays hit sequentially one mirror after the other. For the Montel system (3.19b) a portion of rays coming from the source hit firstly oe1 and secondly oe2, the other portion do the opposite thing. From [LIA$^+$11].

The first step to trace the Montel is that to change the reference frame from the source optical axial to the optical system. This system is chosen to have origin in the centre of whole system with the normal of the two mirror along z and -x axis, as it is showed in Figure 3.13. Moreover, the change of reference frame, has to be done in order to force the beam to have incidence angles, and distance from the centre of the system equal to those chosen by the user. To do this, two rotations and one translation are needed.

The second step is the propagation. The beam can hit any of the two mirrors a new method is implemented. This method, named "*comparison _ time*", compares the time that each ray take to reach each mirror. Calculated the time for each ray, is set a flag that specify the closest optical element. At this point the Beam is divided in three "sub-Beams", a first one that contain the rays going to the first mirror, a second one that contain the rays going to the second mirror, and a third one that contain the rays that, because of the finite size of the mirrors, doesn't hit any mirror. At this point each sub-Beam is traced to the corresponding optical element and so are computed the effect of the mirror on the 1st and 2nd sub-Beams. This process gives three output: "beam1", "beam2" and "beam3". These output contain the information of the beam along the whole propagation system.

The "beam1" and "beam2", are list of two dimension that contain the rays of that will hit the first mirror at the first and at the second iteration. "beam3" is the most important output, because contain the information of the beam at the image plane. This list is divided in three Beam, where the first beam contain the information of the ray that undergo no-reflection, the second Beam contain the information of the ray that undergo one-reflection and the third contain the information of the ray that undergo two-reflections. Figure 3.20, show the image produced by the 3 Beams. The red dots correspond to the beam with no-reflection, the blue dots correspond to the beam with a single-reflection and the green dots correspond to the beam with two-reflection.

The last step of this tracing method consist in a re-change of reference frame to the optical axis of the two reflected beam (as showed in Figure 3.20, where the green dots are centred in the point (0,0)). This transformation is similar to the first step of this tracing method where the two reflection are done with respect to the same angle of incidence, and the translation depend on the value set by the user corresponding to the distance from the centre of the Montel system.

Here below a brief summary of the tracing method:

1. Changing the reference frame from the source optical axis to the Montel system
2. Focus the attention on the travel time of each ray in order to know which is the nearest optical element of each ray
3. free propagation of each ray up to the nearest optical element
4. effect of the system for each ray
5. repeat the 2nd, 3rd and 4th passage two times, in order to consider the two reflection
6. Change the reference system to the optical axes that is subject to two reflection, doing two rotation and one translation
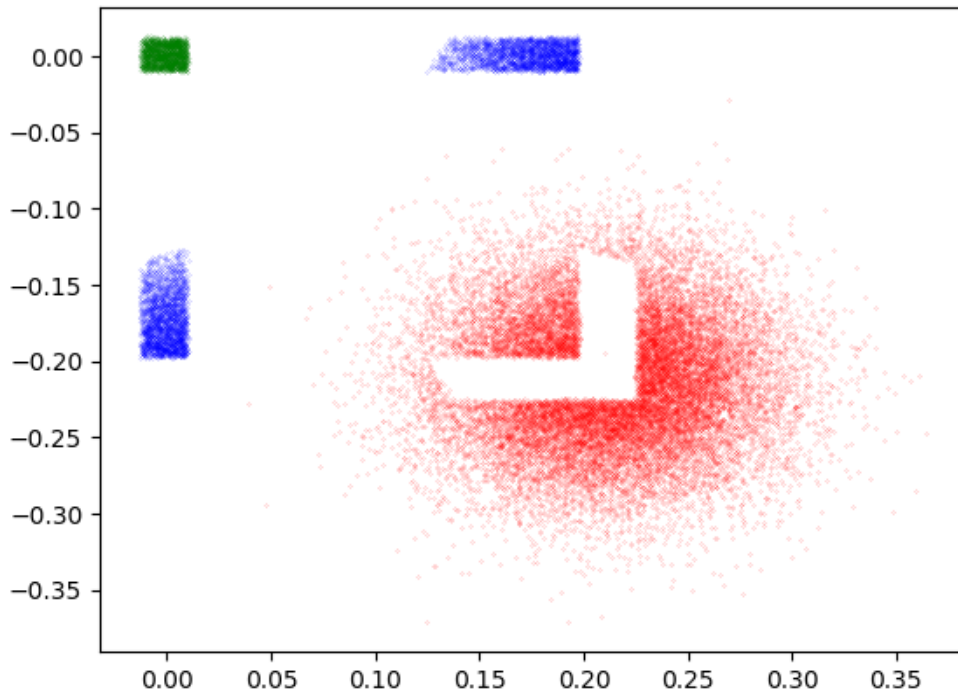
Figure 3.20: Example 8

Because of the importance of the Montel system in my Thesis, it is implemented some additional options with the aim to study better the behaviour of the system. These new parameters that affect the tracing system are:

1. focal distances and incidence angles, that define the two rotation and the translation of the tracing system

2. name of the File in which is saved the data of the simulation, by default no data is saved

3. there is the possibility to choose a different point, from the origin, in which the optical axis hit the system

4. there is also the possibility to have a final output frame that doesn't correspond to the two-reflected beam, but with the non reflected beam or with the other two beam that are reflected only one time

5. It is also the possibility to figure out the footprint of the two reflected beam on the system. For clarity the beam that hit the first mirror and after the second is labelled with red point, the beam that hit the second and after first mirror is labelled by blue colour.

In Chapter 4, these option will be useful in the comprehension of the Montel. The possibilities to change the angle of incidence and to hit different part from the origin can be used to study what happen to a beam when is not aligned, or not perfectly aligned, and use these result to align the system in the laboratories. The possibilities to save a File is useful in particular in those case where there is a huge computational effort that need a lot of time, in these cases is possible to work with

the result of a big simulation without reappointing it, and so save time. Figure 3.21 show the code that trace a Montel elements, containing also the special option that were defined above.

```python
def trace_montel(self, beam, name_file=None, mode=0, p=None, q=None, theta_z=None, theta_x=None, hitting_point=Vector(0., 0., 0.),
                 output_frame=0., print_footprint=1):

    self.oe[0].set_parameters(p=p, q=q, theta=theta_z)
    self.oe[1].set_parameters(p=p, q=q, theta=theta_x)

    v_in = self.get_optical_axis_in(mode)

    self.input_frame(beam, v_in, mode, hitting_point)


    beam1, beam2, beam3 = self.apply_specular_reflections(beam, name_file, print_footprint)

    if output_frame == 0:
        v_out = self.get_optical_axis_out(mode)
    elif output_frame == 1:
        v_out = v_in

    self.output_frame(beam3[0], v_out, mode)
    self.output_frame(beam3[1], v_out, mode)
    self.output_frame(beam3[2], v_out, mode)



    return beam1, beam2, beam3
```

Figure 3.21: Example 9

Chapter 4

Test and Results

In the first part of the Chapter is tested the correct working of the MONWES library. The test for mirrors, ideal lens and KB is done against OASYS software. For the Montel system, because it is not implemented in OASYS, it is done a benchmark with the paper [RKM15].

The second part of the Chapter use the MONWES library to study the behavior of the Montel system. It is studied the effect of a non-centered beam watching what happen to the image dimension and the intensity in the case of centered and non centered beam. At the end it is reported the study that I have done, for the beamline ID20 of the ESRF, of a non-orthogonal Montel mirrors.

4.1 Testing against OASYS

OASYS (OrAnge SYnchrotron Suite) is a graphical environment for optic simulation used in synchrotron facilities based on orange 3, developed by Manuel Sanchez Del Rio (ESRF) and Luca Rebuffi (ELETTRA). The comparison between the program and the OASYS software is done with the system in Figure 4.1. In this system the 1st optical system collimate the source and the 2nd optical system focalize the Beam at the image plane. The different length that characterize the system are: between the source and the 1st optical system there is a distance of $d_1 = f = 0.4m$, between the 1st and the 2nd optical system a distance $d_2 = 0.6m$ and the distance between the 2nd system and the image plane correspond to a distance of $d_3 = f = 0.4$. A system that have parameters defined as before, make a copy of the source image at the image plane. The source parameter used are
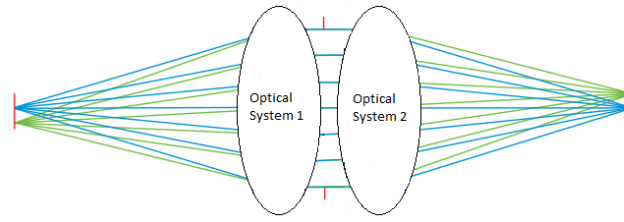
Figure 4.1: Optical system used for the test with OASYS

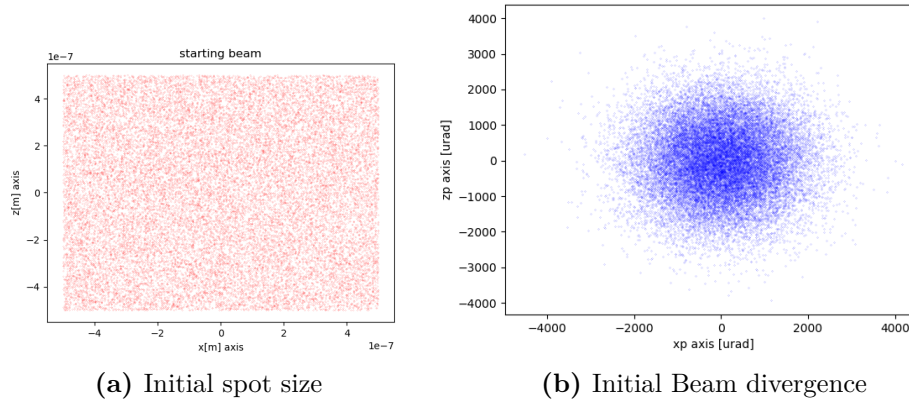**(a)** Initial spot size   **(b)** Initial Beam divergence

Figure 4.2: Parameter of the source used for the test with OASYS

showed in Figure 4.2, and correspond to a square source spot of $1\mu m^2$, and an initial Gaussian divergence with a FWHM of $2.3mrad$. The tests are done using different optical systems, with the same focal length and, for the mirror, with a grazing incidence angle of $\vartheta = 1.719°$. Below are plotted the image of the Beam at the image plane, putting the OASYS results on the right, and my results on the left.

The system simulated are done with:

1. ideal lenses Figure 4.3

2. parabolic mirror Figure 4.4

3. KB system Figure 4.5

As it is showed in the figures 4.3, 4.4 and KB system Figure 4.5, the result, of OASYS and my simulations are in good agreement. The ideal lenses case show a perfect replica of the source image, on the contrary, KB and paraboloid, show similar images but a bit aberrated, because it degrades along the propagation.
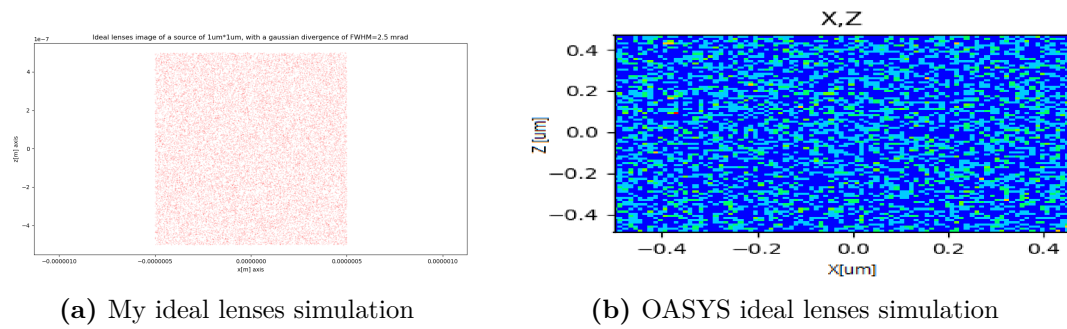
(a) My ideal lenses simulation

(b) OASYS ideal lenses simulation

Figure 4.3: Image for the testing ideal lenses system in Figure 4.1 of: my simulation (Figure 4.3a) and OASYS simulation (Figure 4.3b)
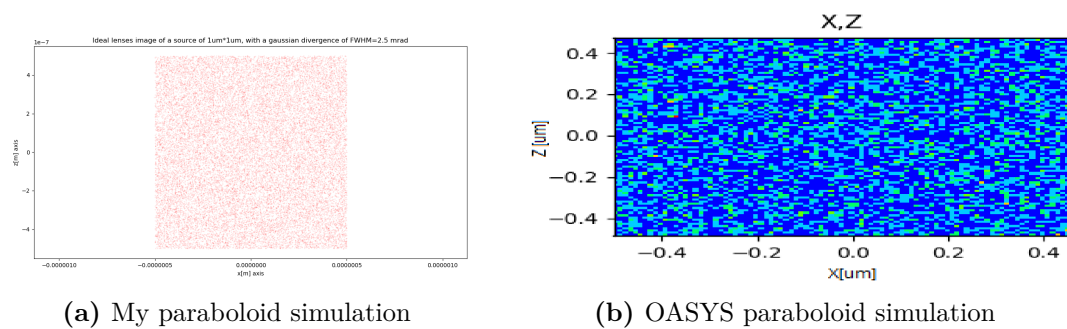

(a) My paraboloid simulation

(b) OASYS paraboloid simulation

Figure 4.4: Image for the testing paraboloid system in Figure 4.1 of: my simulation (Figure 4.4a) and OASYS simulation (Figure 4.4b)

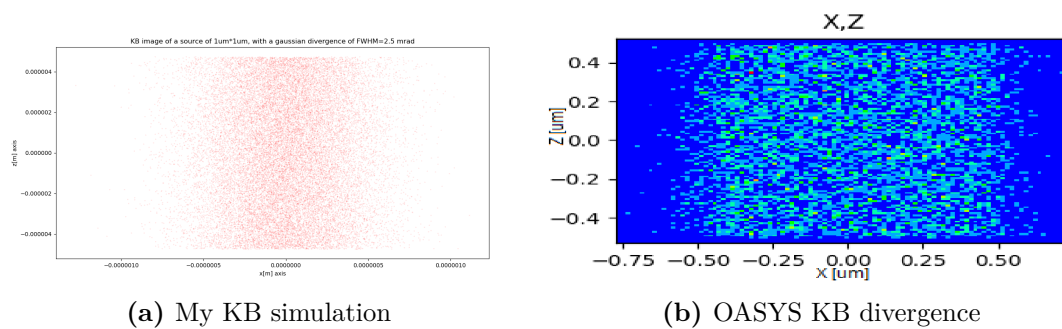
(a) My KB simulation

(b) OASYS KB divergence

Figure 4.5: Image for the testing KB system in Figure 4.1 of: my simulation (Figure 4.5a) and OASYS simulation (Figure 4.5b)
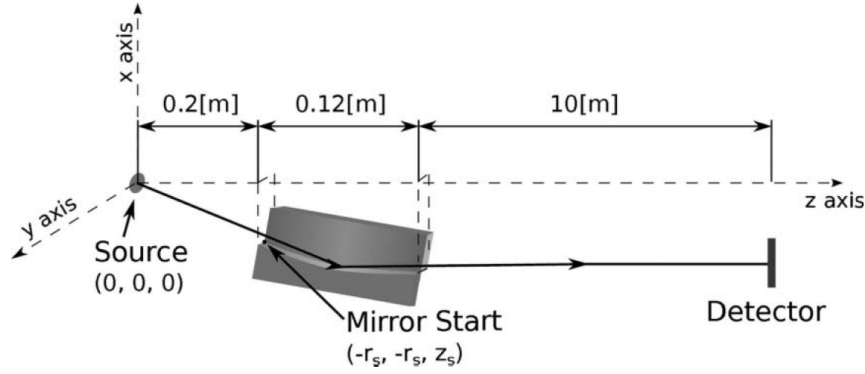
Figure 4.6: Illustration of the Montel system used as a collimator in the paper [RKM15]

4.1.1 Benchmarking

The system used for the benchmarking is showed in Figure 4.6 using the reference frame of the paper [RKM15]. The aim of this system is to collimate a Beam using a Montel with two parabolic mirrors. The source used has a Gaussian dimension of 2.5μm FWHM and a Gaussian divergence of $5mrad$. The distances, between the source/image plane and the center of the Montel are, respectively, $\simeq 0.26$m and 10.06m. The incidence angle of the Beam is $\vartheta_g \simeq 2.86°$. The result, at the image plane, of the beam size and beam divergence, after the double-reflection of the Montel system, is showed in Figure 4.7. There in Figure 4.7a shows the beam at the image plane, and Figure 4.7cshows the divergence. The quantitative values reported on the paper correspond to a Gaussian-like distribution with a spatial FWHM of $\sim$0.7mm for the spot size, and a FWHM of the Gaussian divergence $\sim$ 0.01 mrad.
Repeating the simulation with MONWES, and using the parameter defined in in the paper [RKM15] it obtains Figure 4.7. As it is showed in the Figure 4.7 there are a qualitative good agreement between the two simulation. Also, under a quantitative point of view, there is a good agreement in fact, in my simulation are obtained a value of $\sim$1mm of FWHM of image size, pretty similar to the one of the other simulation, and $\sim$0.01 mrad FWHM of divergence that is equal to the one obtained with the other simulation.

4.2 Analysis of Montel system

In this section a study of the Montel is done, using the Montel tools developed. The first simulation, to verify that Montel work well, study the behaviour of a point-wise source with a certain divergence, using a collimating system. The second simulation, for the same reason of before, simulates a collimating beam with a certain source shape geometry and figure out the image plot obtained by a focalizing system in its image plane. What is expected is a point in the divergence space for the first situation and in the real space for the second simulation, as a consequence of the ideal collimating/focalizing system. For the simulation parabolic Montel with an incidence angle of 2° (the choice of the angle is arbitrary) are used. Parabolic
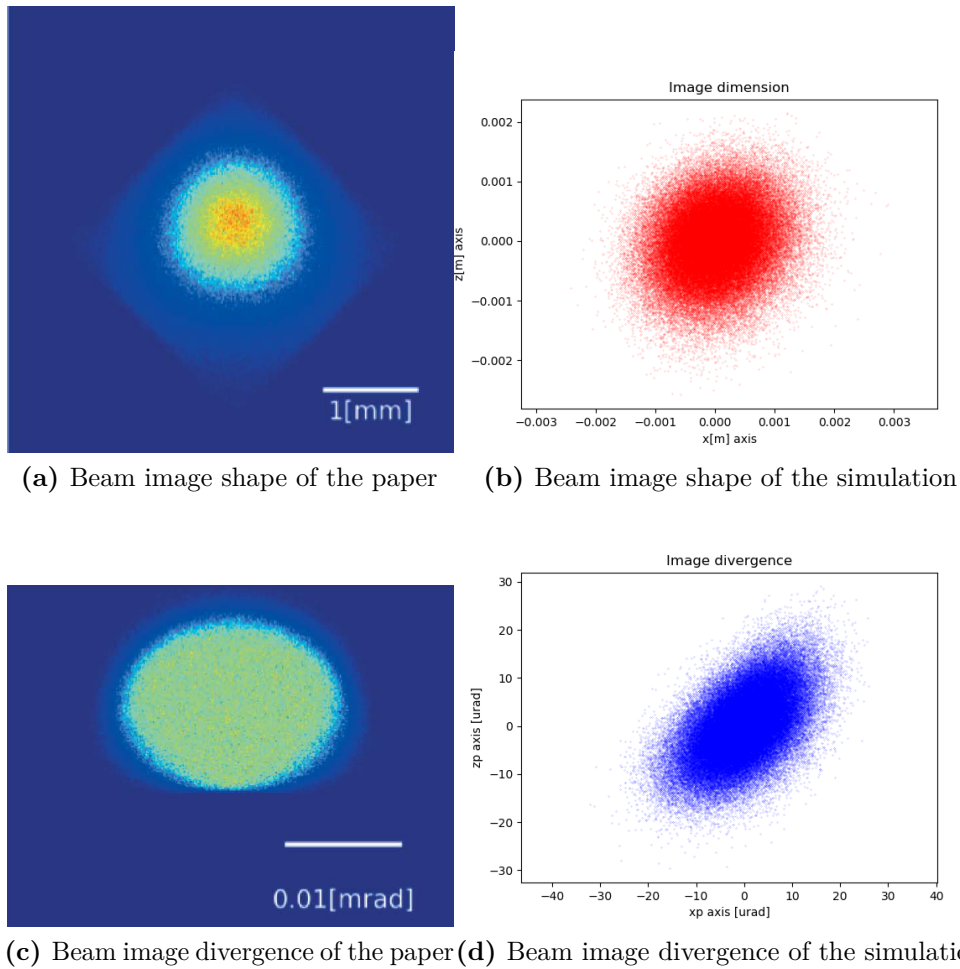
(a) Beam image shape of the paper

(b) Beam image shape of the simulation

(c) Beam image divergence of the paper **(d)** Beam image divergence of the simulation

Figure 4.7: Results of the Montel simulations with a source beam with a FWHM spot of 2.5μm and a Gaussian divergence of 5$mrad$

(a) Source divergence

(b) Image divergence
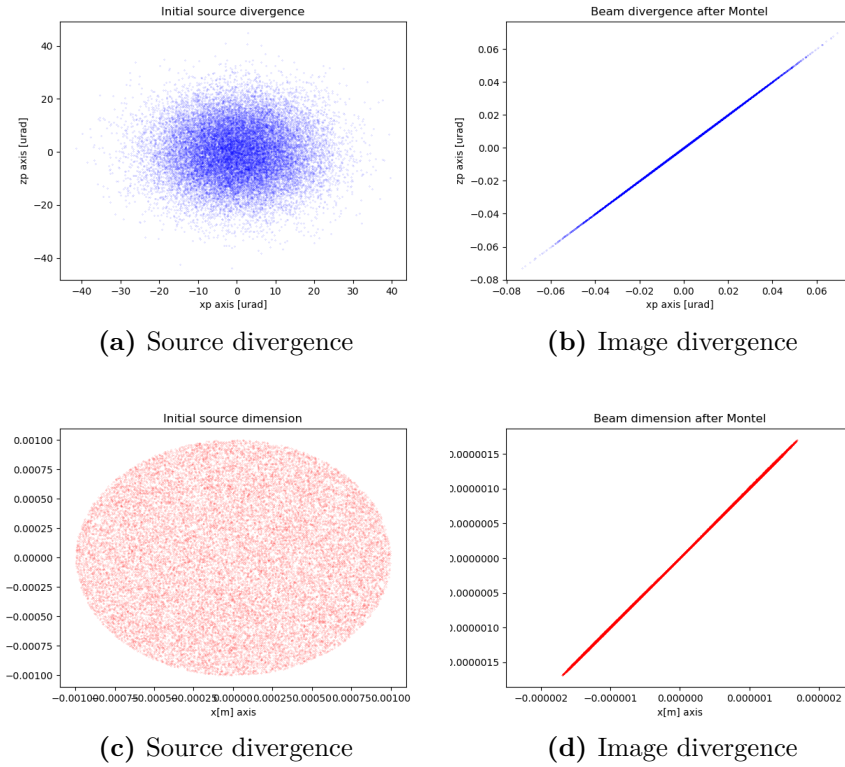
(c) Source divergence

(d) Image divergence

Figure 4.8: Ideal system

system are chosen because is the only way to obtain a perfect collimating Beam. Figure 4.8 reports the result for the ideal collimating/focalizing cases. For the collimation system a point wise source is used with a Gaussian divergence of FWHM of 25μm, 4.8a. At the image plane the Beam (Figure 4.8b) is collimated, reducing its divergence of 3 orders of magnitude. For the focalizing system, it is used a circular source spot having a radius of 1mm, Figure 4.8c, with a collimated source beam. At the image plane the dimension of the Beam (Figure 4.8d) is reduced of 3 order magnitude. It is possible to conclude that both collimating and focalizing system work but not perfectly (the final results are not point). One explanation can be that, because of the particular configuration of the mirrors of the Montel, the effect on the Beam are not perfect. This can be an **intrinsic aberration of the Montel**, that can be studied more in the future.

Up to now the dimension of the Montel were not considered. The Montel is set to have infinite dimension in all the direction. This approach hold in the case of a small source and a narrow profile divergence, that hit only a small part of the system. Otherwise, for example of an isotropic source that can be modelled with a very big divergence, the situation change. In this part, to study to behaviour of a big source, it is used a Beam source with a square shape with a side of 1mm, with a Gaussian profile divergence of FWHM=1mrad. These parameters show what happen to the Montel where it is covered over all its surface. I this case a focalizing parabolic Montel is used with: object distance of 1m, image distance of 3m, incidence angle of 2°, length of the Monte of 0.1m and width of the Montel of
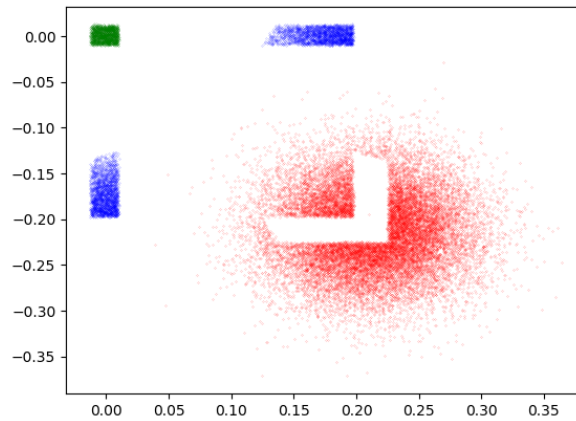
Figure 4.9: Illumination at the image plane of the different Beam (red dots correspond to no-reflected rays, blue dot to one-reflected rays, green dots to two-reflected rays).

20cm. Figure 4.9, show the image plane of the Montel defined above. This plot show 4 figures, the biggest one, represented by the red dots, correspond to the rays that reach the image plane without touch the Montel, the rays coloured in blue, are those which are subject to only one reflection that are positioned in different part of the image plane depending on which mirror meet, those that hit the xy-mirror correspond to the beam elongated along z, the zy-mirror correspond to the beam elongate along x. At the end, the green dots, are the rays that do both reflection and are centred to the center of the image plane by definition of it.

4.3 Non-centred Beam

In this section is studied the effect of a Montel system of a non-centred Beam in order to understand how to align correctly beam. The alignment study is study simulating a beam that hit different point of the Montel. Is reported the behaviour about the change of FWHM of both $x^{'}$ and $z^{'}$, of a small ($1\mu m^2$) source with a narrow divergence ($25\mu rad$), following different path. Figure 4.10 show the different path followed to simulate the non-centred. Every path is labelled with a name:

1. Y

2. XZ

3. XYZ1

4. XZY2

The system used is a focalizing parabolic Montel with an object focal distance of 0.2m and an image focal distance of 0.9, working on mirror designed for incidence angle of $\vartheta_g = 2°$. Figure 4.11 show the result the two FWHM of the beam changing the incidence point of the beam moving the different paths. This point is defined
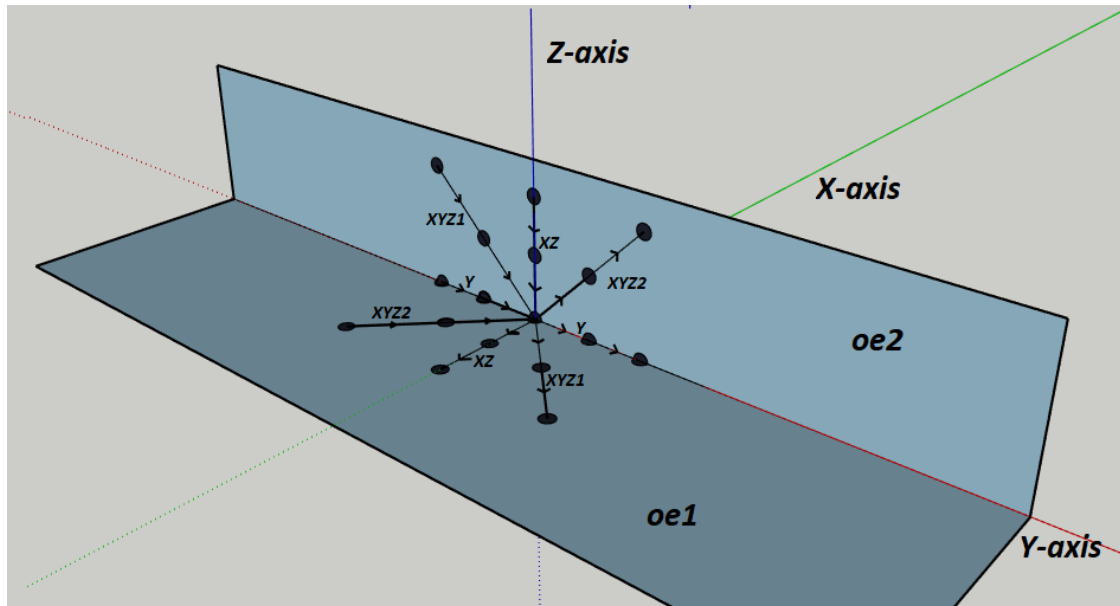
Figure 4.10: Different path for simulate the non-centred beam

with respect to the center of the Montel system that correspond to the origin (0, 0, 0). In Figure 4.12a, the incidence point move along y-axis, start from the point (0, 1.5mm, 0) and arriving to the point (0, -1.5mm, 0), and show, more or less, a flat behaviour of the FWHM. Figure 4.12b start from the point (0, 0, 0.15mm) and arrive to (-0.15mm, 0, 0) and have specular behaviour for the two FWHM, there is a minimum of the two FWHM near the origin point, moving on the oe1 worse the FWHM of z' and maintain the other constant, on the contrary, moving on the oe2 the situation is reversed, in this case the FWHM of x' get worse, maintaining constant the one of z'. Figure 4.12c start from (0, 1.5mm, 0.15mm) and arrive to (-0.15mm, -1.5mm, 0) and Figure 4.12d start from (-0.15mm, 1.5mm, 0) and arrive to (0., -1.5mm, 0.15mm). The behaviour of this last two path are similar to that of 4.12b, this is reasonable, because the motion along y-axis does not influence the FWHM because of the definition of the cylindrical mirror, that in any point along the y direction have the same geometry.

In Figure 4.12 it is show the intensity profile of the two-reflection beam of source with a $10mm^2$ of area and a Gaussian divergence of FWHM $= 25\mu rad$. In this case the Montel used is the same as before but with a length of 20cm and a width of 2cm. The intensity is calculated as the number of the rays in the two-reflection beam with respect to the initial number of rays. The different path move along these points; ymax=50cm, ymin=-50cm, xmin=-2cm, xmax=0, zmax=2cm, zmin=0 The plots in Figure 4.12, are interesting, because represents the intensity of the "green" Beam in Figure 4.9, that can be directly measured and so, it is possible to relate the centring of the Beam calculating the intensity of this Beam.
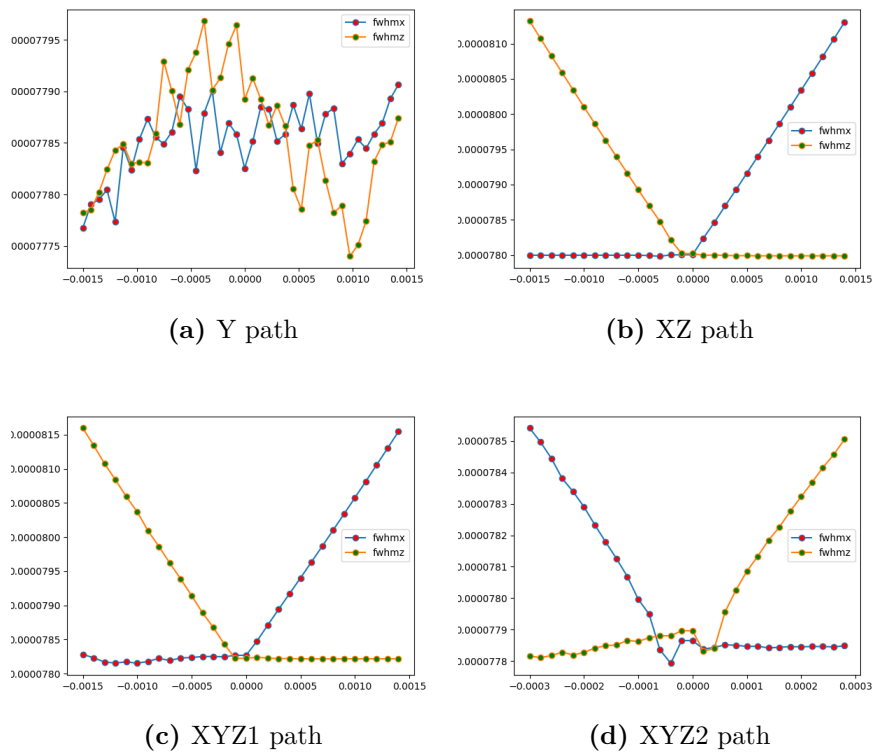
(a) Y path

(b) XZ path

(c) XYZ1 path

(d) XYZ2 path

Figure 4.11: Results of the changing of the x and z FWHM at the image following different path defined in Figure 4.10. The Montel system used have a source beam with a FWHM spot of 2.5μm and a Gaussian divergence of $5mrad$

(a) Y path

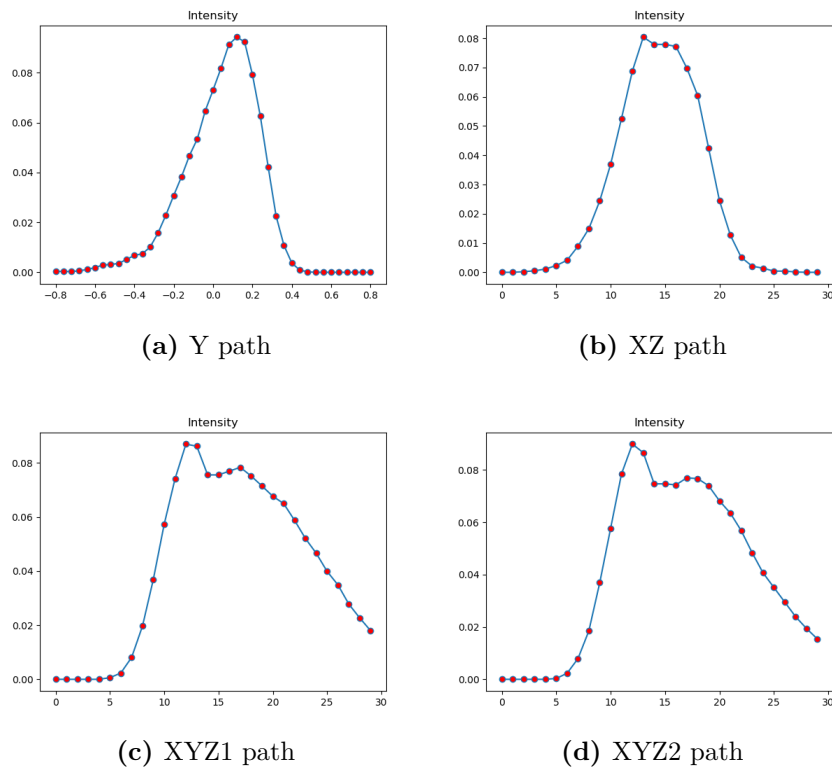**(b)** XZ path

(c) XYZ1 path

(d) XYZ2 path

Figure 4.12: Change of the intensity depending on the path defined in Figure 4.10. The Montel system used have a square spot of $10mm^2$ and a Gaussian divergence of $25mrad$

4.4 Simulation of a Montel system for ID20

In this section is reported the study that I have done for the beam of ID20 of the ESRF. The simulation were done in order to study the Montel system bought as analyser that will be used in the beamline. The purpose of this analyser is to collimate the radiation in entrance. Company information states that changing the orthogonality, with a particular angle, of the mirrors brings a better collimation of the Beam.

4.4.1 System parameters

The system simulated have a source size of $1\mu m^2$(see Figure 4.13a) with a Gaussian divergence of $25\mu rad$(see Figure 4.13b). The parameters of the system are: object distance of $351mm$, mirror Length of $300mm$, mirror width of $100mm$, the error max between the orthogonal configuration of the two mirror is of $\Delta = \pm 0.03°$ and an incidence angle of $18.1mrad$. In Figure 4.14 is showed a 3D graphic view of the Monter system with the parameter used.
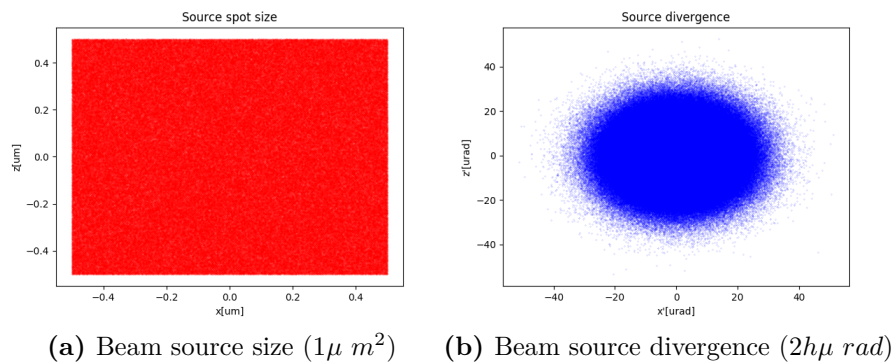

(a) Beam source size $(1\mu\ m^2)$ (b) Beam source divergence $(2h\mu\ rad)$

Figure 4.13: Source parameters used for the study of the Montel Analyser for ID20
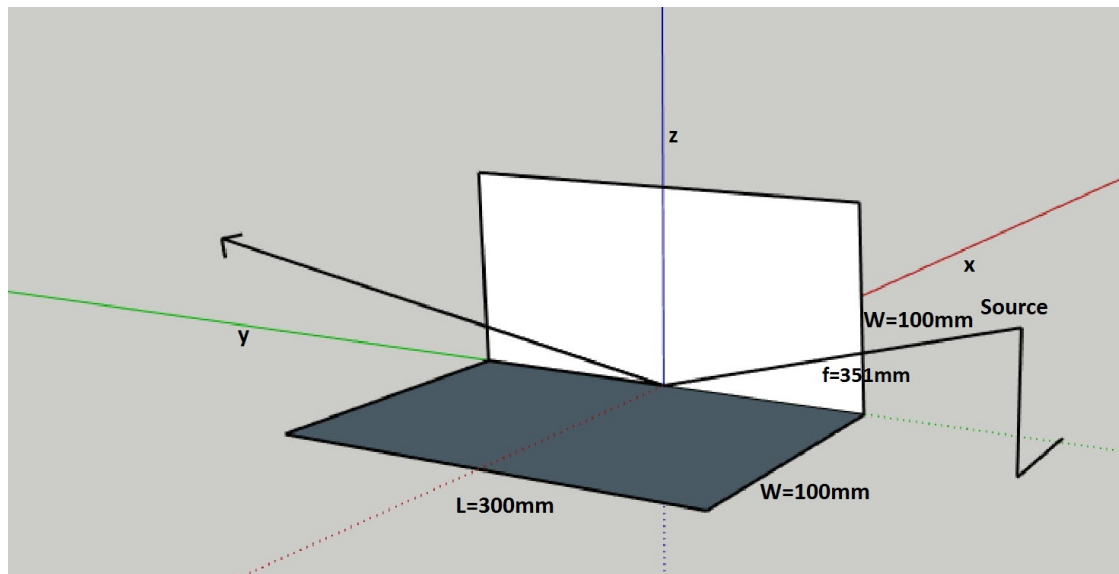
Figure 4.14: Montel parameters used for the simulation for ID20

4.4.2 Result of beam figure and footprint

The image plane is positioned at $1m$ from the center of the Montel system. The property of the beam at the image plane are showed in Figure **??**.It is obtained, a new spot size with a length of $60\mu\ m$ in the x direction and $100\mu\ m$ in the z direction, and the divergence has a dimension of $\simeq 40\mu\ rad$.
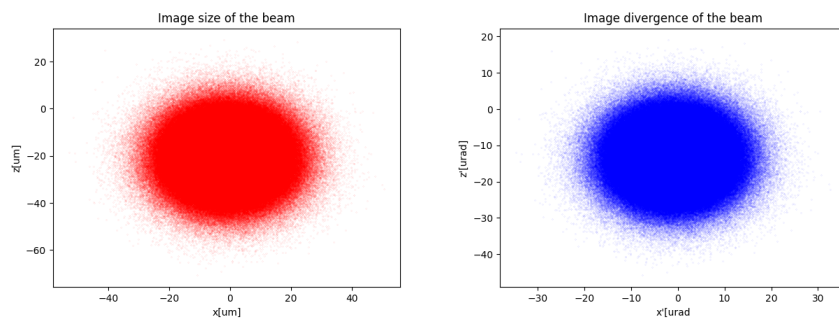
(a) Size of the Beam at the image plane **(b)** Divergence of the Beam at the image plane

Moreover is interesting to note the footprint of the two mirror (Figure 4.15) because the area hit by the beam have a greater component on the y direction (due to the grazing incidence), than in the other direction.The x-length of the xy-mirror, and the z-length of the zy-mirror, is very small (at the order of $20\mu\ m$) with respect to the y-length that is $\simeq 20mm$.
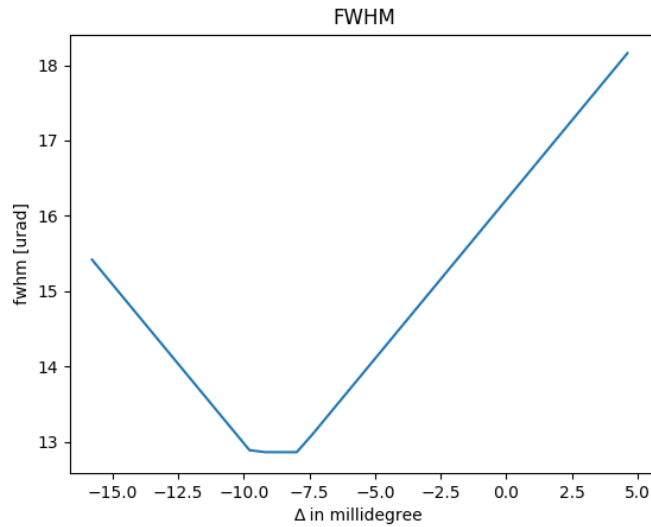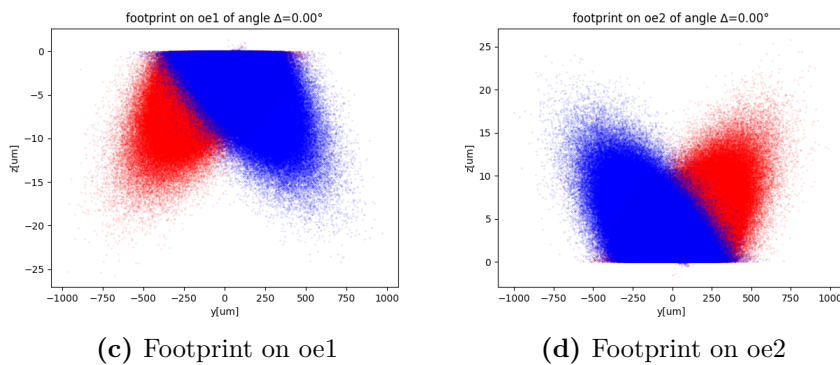
**Figure 4.16:** FWHM of x' after the Montel changing the orthogonality

(c) Footprint on oe1

(d) Footprint on oe2

Figure 4.15: Footprint, on the xy-mirror (4.15c) and on zy-mirror (4.15d). The red dots are those rays that hit before xy-mirror and after zy-mirror, the blue ones hit first xy-mirror and after zy-mirror.

4.4.3 Analysis of orthogonality

Figure 4.17 presents the interesting histograms versus the horizontal anlge x' when the angle between the mirrors change ($\alpha = 90° + \Delta$). It can be noted a improvement of the collimation of the beam changing the angle in the case of closer mirrors ($\Delta = -0.01°$). Figure 4.16 show the trend of the FWHM of the x' changing the angle Δ, it is possible to note a minimum for negative angle (this ideal situation is the pink curve reported in Figure 4.17) after that the situation become worse. Moreover, the behaviour of the FWHM is not symmetrical with respect to 0°, in case of negative angle deviation the situation improve for a small range of deviation angle, after that, the trend get worse, on the opposite way, the situation get worse increasing the positive deviation angle.
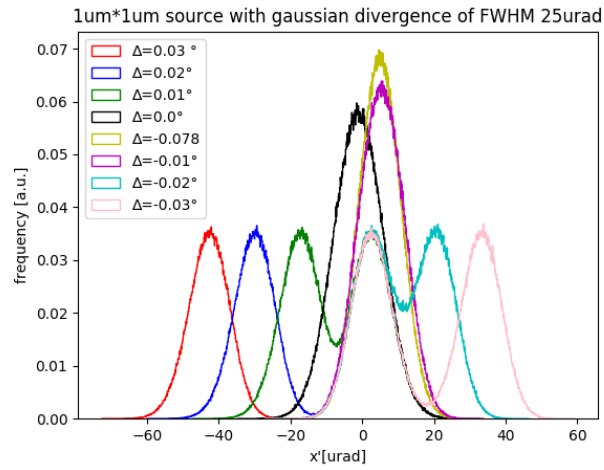
(a) Real histogram
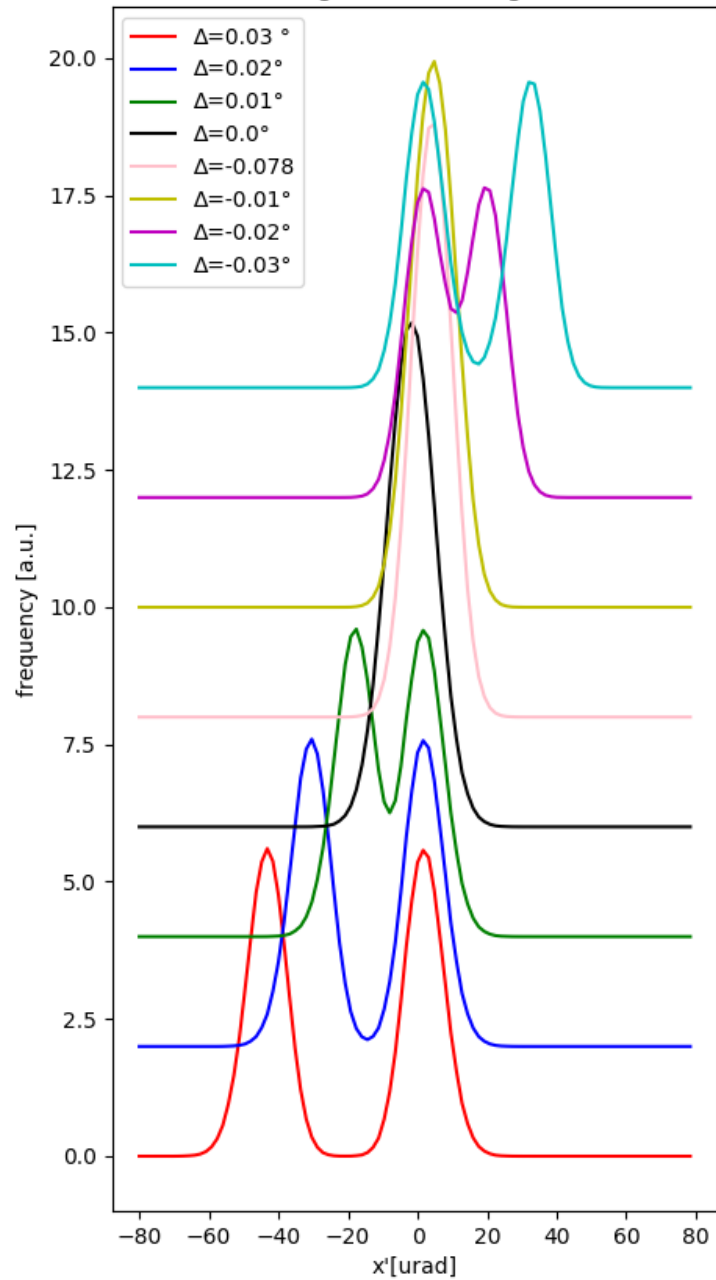
Conclusioni

In this thesis I have presented the reason why conical mirrors at grazing incidence are used for X-ray radiation. With a focus on the Montel system. After, I have described the implementation method for the python library MONWES that will implement the Montel system into the OASYS Graphical Environment. The tests done against OASYS, for elements already existing, and the benchmarking with [RKM15] show the correct working of the program.

The simulation done on Montel, shows an intrinsic aberration. Due to the kind of mirror disposition the image cannot be focused perfectly. On the contrary using a mirrors disposition such as in KB system it is obtained the ideal situation. This aberration is due to the fact on the orthogonal disposition of the mirrors. There is no way to dispose the Beam on the mirrors in order to cancel out this aberration. Moreover, on the study done for ID20, it can be concluded that the information provided by the company are similar to the ones obtained with the simulation. Having a less orthogonal mirrors can improve the collimating effect of the Montel. The code is still under development, it is still missing the Wolter system. It is also possible to improve the library including the angle-dependant reflection factor. In the future, after the integration with OASYS, it can be used to designing beamlines that use Montel system.

Appendix A

How to calculate the ellipse's and hyperbola's coefficients

A.1 Ellipse

For the ellipse showed in Figure A.1, the ellipse is defined as:

$$\left(\frac{x'}{a}\right)^2 + \left(\frac{y'}{b}\right)^2 = 1 \tag{A.1}$$

with

$$c^2 = a^2 - b^2 \tag{A.2}$$

Because the ellipse is the curve in a plane surrounding two focal points such that the sum of the distances to the two focal points is constant for every point, so:

$$p + q = (c + a) + (a - c) = 2a \tag{A.3}$$

Thus

$$a = \frac{p + q}{2} \tag{A.4}$$

Now, considering the triangle $AA'P$, using the law of cosines, and substituting with the equations above:

$$4c^2 = p^2 + q^2 - 2pq\cos(2\vartheta) \tag{A.5}$$

$$4(a^2 - b^2) = p^2 + q^2 - 2pq\cos(2\vartheta) \tag{A.6}$$

$$(p + q)^2 - 4b^2 = p^2 + q^2 - 2pq\cos(2\vartheta) \tag{A.7}$$

$$b^2 = \frac{2pq(1 + \cos(2\vartheta)}{4} \tag{A.8}$$

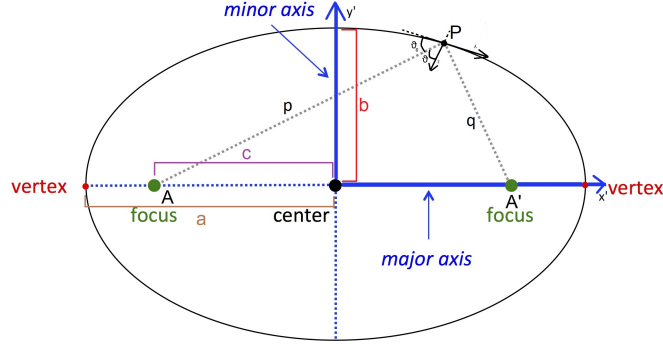$$b = \sqrt{pq}\cos(\vartheta) \tag{A.9}$$

Figure A.1: Ellipse's system

A.2   Hyperbola

For the Hyperbola the situation is similar. For the system in Figure A.2, the equation of the parabola is

$$\left(\frac{x'}{a}\right)^2 - \left(\frac{y'}{b}\right)^2 = 1 \tag{A.10}$$

with

$$c^2 = a^2 + b^2 \tag{A.11}$$

In this case the definition of hyperbola is the curve in a plane surrounding two focal points such that the difference of the distances to the two focal points is constant for every point, so:

$$p - q = (c + a) - (c - a) = 2a \tag{A.12}$$

Thus

$$a = \frac{p - q}{2} \tag{A.13}$$

As before, considering the triangle $F_1 F_2 P$, using the law of cosines, and substituting with the equations above:

$$4c^2 = p^2 + q^2 - 2pq\cos(2\vartheta_g) \tag{A.14}$$

$$4(a^2 + b^2) = p^2 + q^2 - 2pq\cos(2\vartheta_g) \tag{A.15}$$

$$(p - q)^2 + 4b^2 = p^2 + q^2 - 2pq\cos(2\vartheta_g) \tag{A.16}$$

$$b^2 = \frac{2pq[1 - \cos(2\vartheta_g)]}{4} \tag{A.17}$$

$$b = \sqrt{pq}\sin(\vartheta_g) = \sqrt{pq}\cos(\vartheta) \tag{A.18}$$
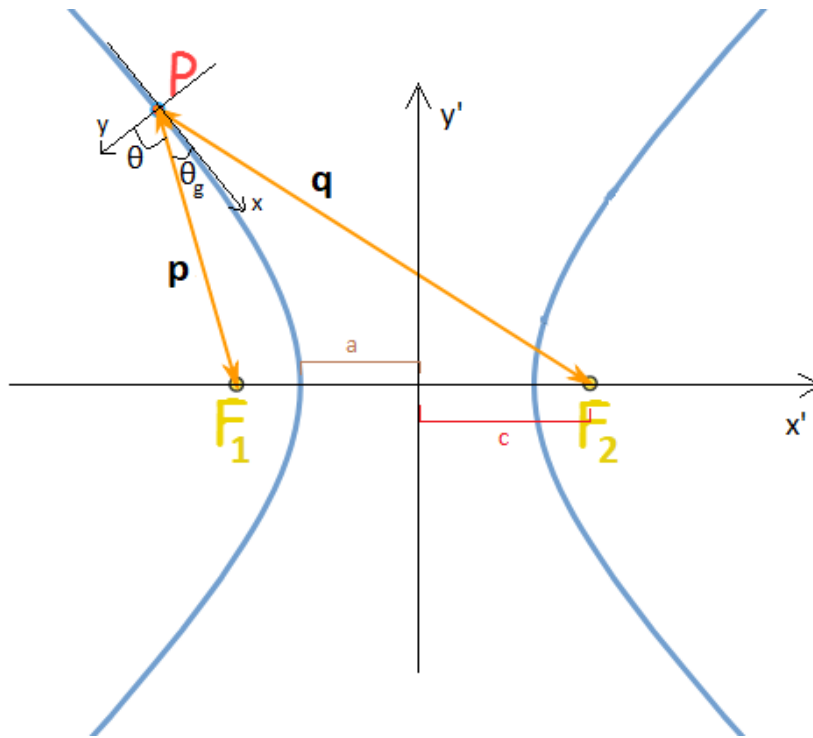
Figure A.2: Hyperbola's system

Bibliography

[Aga91]   Bipin K Agarwal. Interaction of x-rays with matter. In *X-Ray Spectroscopy*, pages 121–126. Springer, 1991.

[BAR11]   Ray BARRETT. X-ray optics for synchrotron radiation beamlines. Presentation of Ray Barrett on his work at ESRF presented at ESI2011: 2nd EIROforum School on Instrumentation, 2011.

[Bra97]   Joseph JM Braat. Abbe sine condition and related imaging conditions in geometrical optics. In *Fifth International Topical Meeting on Education and Training in Optics*, volume 3190, pages 59–65. International Society for Optics and Photonics, 1997.

[CL70]   Don T Cromer and David Liberman. Relativistic calculation of anomalous scattering factors for x rays. *The Journal of Chemical Physics*, 53(5):1891–1898, 1970.

[CMW16]   Shenghao Chen, Shuang Ma, and Zhanshan Wang. Wolter-i-like x ray telescope structure using one conical mirror and one quadric mirror. *Chinese Optics Letters*, 14(12):123401, 2016.

[Dal16]   Daniele Dallacasa. Processi di radiazione e mhd, 2016.

[dRRD$^+$14]   Manuel Sanchez del Rio, Luca Rebuffi, Janez Demsar, Niccolo Canestrari, and Oleg Chubar. A proposal for an open source graphical environment for simulating x-ray optics. In *Advances in Computational Methods for X-Ray Optics III*, volume 9209, page 92090X. International Society for Optics and Photonics, 2014.

[Fit06]   Richard Fitzpatrick. Rayleigh scattering, 2006.

[FTGY$^+$00]   Robert Edward Fischer, Biljana Tadic-Galeb, Paul R Yoder, Ranko Galeb, Bernard C Kress, Stephen C McClain, Tom Baur, Richard Plympton, Bob Wiederhold, and Bob Grant Alastair J. *Optical system design*. Citeseer, 2000.

[GHJV95]   Erich Gamma, Richard Helm, Ralph Johnson, and John Vlissides. *Design patterns: Abstraction and reuse of object-oriented design*. Springer, 1995.

[gis15]   gisaxs. Refractive index, 2015.

[HHK+10]   Marcelo Goncalves Honnicke, Xianrong Huang, Jeffrey W Keister, Chaminda Nalaka Kodituwakku, and Yong Q Cai. Tracing x-rays through an l-shaped laterally graded multilayer mirror: a synchrotron application. *Journal of synchrotron radiation*, 17(3):352–359, 2010.

[IBK09]   Gene E Ice, Rozaliya I Barabash, and Ali Khounsary. Nested mirrors for x-rays and neutrons. In *Advances in X-Ray/EUV Optics and Components IV*, volume 7448, page 74480B. International Society for Optics and Photonics, 2009.

[KB48]   Paul Kirkpatrick and Albert Vincio Baez. Formation of optical images by x-rays. *JOSA*, 38(9):766–774, 1948.

[LBN10]   MSD LBNL. Center for x-ray optics, 2010.

[LIA+11]   Wenjun Liu, Gene E Ice, Lahsen Assoufid, Chian Liu, Bing Shi, Ruben Khachatryan, Jun Qian, Paul Zschack, Jonathan Z Tischler, and J-Y Choi. Achromatic nested kirkpatrick–baez mirror optics for hard x-ray nanofocusing. *Journal of synchrotron radiation*, 18(4):575–579, 2011.

[Man81]   Steven T Manson. Theory of sub-kev photoionization cross sections. In *AIP Conference Proceedings*, volume 75, pages 156–161. AIP, 1981.

[Mic86]   A.G. Michette. *Optical systems for soft X rays*. Plenum Press, 1986.

[Mon57]   M i Montel. X-ray microscopy with catamegonic roof mirrors. *X-ray Microscopy and Microradiography*, pages 177–185, 1957.

[MSL+14]   K Mundboth, J Sutter, D Laundy, S Collins, S Stoupin, and Yu Shvyd'ko. Tests and characterization of a laterally graded multilayer montel mirror. *Journal of synchrotron radiation*, 21(1):16–23, 2014.

[MY09]   S Matsuyama and H Yumoto. Textbook for hard x-ray focusing with kirkpatrick-baez optics. *Unpublished Report*, 2009.

[RdR17a]   Luca Rebuffi and Manuel Sanchez del Rio. Interoperability and complementarity of simulation tools for beamline design in the oasys environment. In *Advances in Computational Methods for X-Ray Optics IV*, volume 10388, page 1038808. International Society for Optics and Photonics, 2017.

[RdR17b]   Luca Rebuffi and Manuel Sanchez del Rio. Oasys (orange synchrotron suite): an open-source graphical environment for x-ray virtual experiments. In *Advances in Computational Methods for X-Ray Optics IV*, volume 10388, page 103880S. International Society for Optics and Photonics, 2017.

[RKM15]   Giacomo Resta, Boris Khaykovich, and David Moncton. Nested kirkpatrick–baez (montel) optics for hard x-rays. *Journal of Applied Crystallography*, 48(2):558–564, 2015.

[ro]   X ray optic. Curved mirror optics.

[SFV09]   Francesc Salvat and José Fernández-Varea. Overview of physical
            interaction models for photon and electron transport used in monte
            carlo codes. *Metrologia*, 46:S112, 03 2009.

[Sin11]   Kulinder Pal Singh. Grazing incidence optics for x-ray astronomy.
            Journal of Optics, 40(3):88, 2011.

[SS05]   Robert Shannon and Roland Shack. *Legends in Applied Optics*. James
            E. Harvey, 2005.

[Tel]   TelescopeOptics. Conics and aberrations.

[Uni16]   Boston University. *Compton Scattering*, 2016.

[Wik18]   Wikipedia. Parabola (geometria). 2018. [Online; accessed 1-December-
            2018].

[Wol75]   Hans Wolter. Mirror systems with grazing incidence as image-
            forming optics for x-rays. *Mirror systems with grazing incidence as
            image-forming optics for X-rays Transl. into ENGLISH from Ann.
            Phys.(Leipzig), ser. 6, v. 10, 1952 p 94-114*, 1975.